

See discussions, stats, and author profiles for this publication at: <https://www.researchgate.net/publication/5274271>

Inner-Sphere Mechanism for Molecular Oxygen Reduction Catalyzed by Copper Amine Oxidases

ARTICLE *in* JOURNAL OF THE AMERICAN CHEMICAL SOCIETY · AUGUST 2008

Impact Factor: 12.11 · DOI: 10.1021/ja801378f · Source: PubMed

CITATIONS

37

READS

29

7 AUTHORS, INCLUDING:



[Arnab Mukherjee](#)

Johns Hopkins University

10 PUBLICATIONS 152 CITATIONS

[SEE PROFILE](#)



[David M Dooley](#)

University of Rhode Island

168 PUBLICATIONS 5,288 CITATIONS

[SEE PROFILE](#)



[Justine P Roth](#)

Johns Hopkins University

55 PUBLICATIONS 1,240 CITATIONS

[SEE PROFILE](#)

Published in final edited form as:

J Am Chem Soc. 2008 July 23; 130(29): 9459–9473. doi:10.1021/ja801378f.

An Inner-Sphere Mechanism for Molecular Oxygen Reduction Catalyzed by Copper Amine Oxidases

Arnab Mukherjee[‡], Valeriy V. Smirnov[‡], Michael P. Lanci[‡], Doreen E. Brown[†], Eric M. Shepard[†], David M. Dooley[†], and Justine P. Roth^{‡*}

[‡]Department of Chemistry, Johns Hopkins University, 3400 North Charles St., Baltimore, MD 21218

[†]Department of Chemistry and Biochemistry, Montana State University, Bozeman, MO 59717

Abstract

Copper and topaquinone (TPQ) containing amine oxidases utilize O₂ for the metabolism of biogenic amines while concomitantly generating H₂O₂ for use by the cell. The mechanism of O₂ reduction has been the subject of long-standing debate due to the obscuring influence of a proton-coupled electron transfer between the tyrosine-derived TPQ and copper, a rapidly established equilibrium precluding assignment of the enzyme in its reactive form. Here we show that substrate-reduced pea seedling amine oxidase (PSAO) exists predominantly in the Cu^I, TPQ semiquinone state. A new mechanistic proposal for O₂ reduction is advanced on the basis of thermodynamic considerations together with kinetic studies (at varying pH, temperature and viscosity), the identification of steady-state intermediates and the analysis of competitive oxygen kinetic isotope effects: ¹⁸O KIEs, [*k*_{cat}/*K*_M(^{16,16}O₂)]/[*k*_{cat}/*K*_M(^{16,18}O₂)]. The ¹⁸O KIE = 1.0136 ± 0.0013 at pH 7.2 is independent of temperature from 5 to 47°C and insignificantly changed to 1.0122 ± 0.0020 upon raising the pH to 9, thus indicating the absence of kinetic complexity. Using density functional methods, the effect is found to be precisely in the range expected for reversible O₂ binding to Cu^I to afford a superoxide, [Cu^{II}(η¹-O₂)^{-I}]⁺, intermediate. Electron transfer from the TPQ semiquinone follows in the first irreversible step to form a peroxide, Cu^{II}(η¹-O₂)^{-II}, intermediate driving the reduction of O₂. The similar ¹⁸O KIEs reported for copper amine oxidases from other sources raise the possibility that all enzymes react by related inner-sphere mechanisms although additional experiments are needed to test this proposal.

Introduction

Copper amine oxidases¹ belong to family of related quinoproteins which use molecular oxygen to effect oxidative deamination of primary amines to aldehydes and concomitantly produce hydrogen peroxide. The H₂O₂ is believed to have vital physiological as well as pathophysiological roles, particularly in cell signaling, inflammation and diseases of the connective tissue.²⁻⁴ The efficacy of H₂O₂ production is controlled by the enzyme's ability to mediate electron transfer from its reduced quinocofactor, which is derived from post-translational modification of an active site tyrosine.^{1d} Remarkably, the enzymic rate of electron transfer to O₂ exceeds that of structurally analogous phenolic compounds in solution by several (>10⁵) orders of magnitude.

E-mail: jproth@jhu.edu.

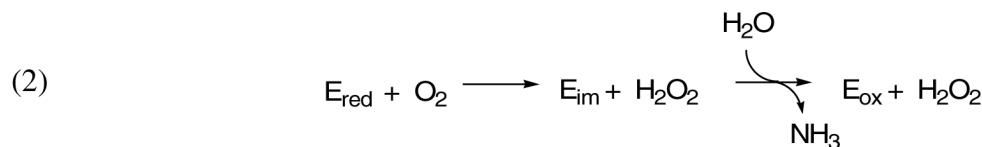
Supporting Information Available: Includes details concerning the methods used to calculate oxygen isotope effects, graphics showing the minimum energy structures and molecular orbitals as well as list of the complete set of computed vibrational frequencies for each structure. This information is available free of charge on the world wide web at <http://pubs.acs.org>.

As with many proteins that contain redox active organic cofactors and metal ions, the origins of catalytic acceleration in reactions with O₂ have been a challenge to understand. The ambiguity in copper amine oxidase catalysis derives largely from an internal redox equilibrium which complicates assignment of the reactive form. Nevertheless, much effort has been devoted to studying the mechanisms of O₂ activation.⁵ These investigations provide valuable insights as to the strategies used by enzymes to catalyze oxidations while avoiding damage by reactive oxygen species.^{5a} The connection between oxidative damage and enzymes is becoming increasingly clear with copper-containing oxidases^{2,4,6} as well as superoxide dismutases⁷ being implicated in degenerative diseased states. The underlying mechanisms by which the enzymes are damaged possibly involve self-generated reactive oxygen species and remain only marginally understood.

In this work, we address the reductive activation of O₂ mediated by copper amine oxidase and the origins of the catalytic rates. In such metalloenzymes, O₂ reactivity can occur by either inner-sphere or outer-sphere electron transfer (ET) and combinations thereof. In inner-sphere ET, a bond between the redox metal and O₂ is formed in the transition state; whereas in outer-sphere ET, the reactant coordination geometries remain unchanged and O₂^{•−} is produced as an intermediate prior to binding to the metal.⁸ The coordination geometry of the metal and amino acids lining the active site influence the kinetic and thermodynamic barriers which differentiate the ET pathways. Yet the factors that make one mechanism preferred over another have been difficult to define in the absence of the appropriate physical probes. Outlined in this study, is the application of competitive oxygen kinetic isotope effects together with density functional methods as a potential solution to this problem.

The present study focuses specifically on the copper amine oxidase from pea seedling (PSAO) and the question of whether structurally homologous eukaryotic enzymes catalyze the reduction of O₂ to H₂O₂ by a common mechanism.⁹ All members of the copper amine oxidase family contain a topaquinone (2,4,5-trihydroxyphenylalanine quinone, TPQ) cofactor in each homodimeric subunit. The TPQ is derived from oxidation of a specific tyrosine¹ via a self-processing reaction that utilizes O₂ while exploiting the electronic structure of the copper ion and the hydrogen bond network of the active site,¹⁰ factors which are also expected to influence the enzyme's catalytic reaction with O₂.

Catalysis in PSAO can be separated into kinetically independent reductive and oxidative half-reactions according to a ping-pong kinetic mechanism.¹¹ During the reductive phase (Eq 1), two electrons are transferred from the amine to the oxidized enzyme (E_{ox}) which contains topaquinone, TPQ_{ox}, and Cu^{II}. This reaction involves conversion of a substrate Schiff-base to a product Schiff-base upon C–H deprotonation by a conserved aspartate residue.¹² Hydrolysis and product release afford the reduced enzyme (E_{red}) initially containing TPQ_{red} and Cu^{II}. This reduced state generates a neutral semiquinone, TPQ_{sq}, and Cu^I via an internal proton-coupled electron transfer. Equilibrium mixtures of TPQ_{sq}/Cu^I and TPQ_{red}/Cu^{II} are formed in enzymes from various sources with the relative concentrations spanning a wide range. Data obtained in this study reveal that E_{red} in PSAO consists of ~80% TPQ_{sq}/Cu^I at physiological pH (*vide infra*). This species, assuming its kinetic competence, would likely be involved in the oxidative phase of catalysis (Eq 2), where two reducing equivalents are transferred from E_{red} to O₂ forming H₂O₂ and the enzyme iminoquinone (E_{im}).



The presence of electronically-coupled,¹³ redox-active cofactors complicates the study of the O₂ reduction mechanism. Crystal structures¹⁴⁻¹⁶ reveal that the Cu^{II} and TPQ_{ox} in the E_{ox} lie within ~6 Å and are connected by hydrogen bonds which vary depending on the orientation of the organic cofactor. The two E_{ox} structures shown in Figure 1 are related by rotation of TPQ_{ox} 180° about C_α-C_β. Only the HPAO structure is believed to be in a configuration conducive to the reductive half-reaction with Asp319 positioned to act as a base.¹² Whether the alternate structure of E_{ox} in PSAO is also favored in E_{red} or capable of reacting with O₂ in the oxidative half-reaction has not been understood.

The intricate hydrogen-bonding within the copper amine oxidase active sites might facilitate coupled movements of electrons and protons in a single step. This type of proton-coupled electron transfer reaction can lower barriers to redox processes that would otherwise require formation of high-energy, charged intermediates. In PSAO, the rapid oxidation of TPQ_{red} by Cu^{II} results in an equilibrium (*K*_{int}) that is established on the timescale of microseconds.¹⁷ As a result, the TPQ_{sq}/Cu^I state is kinetically competent to sustain catalysis in this particular enzyme. In the potentially reactive form, the TPQ_{sq} is inert to oxygenation while the Cu^I is expected to be highly reactive towards O₂.¹⁸

This is, to the best of our knowledge, the first detailed investigation of the O₂ activation mechanism in PSAO. Attempts to correlate the steady-state kinetics to the internal redox equilibrium are described as are experiments that probe the contributions of proton and electron transfer to the observed bimolecular rate constant, *k*_{cat}/*K*_M(O₂). The contribution of common steps within *k*_{cat}/*K*_M(O₂) and *k*_{cat} is examined through the analysis of substrate deuterium kinetic isotope effects and the intermediates which accumulate during steady-state turnover with fast and slow substrates.

Competitive oxygen kinetic isotope effects (¹⁸O KIEs) on reactions of natural abundance O₂, *k*_{cat}/*K*_M(^{16,16}O₂)/*k*_{cat}/*K*_M(^{16,18}O₂), are prominently featured in this study. These values have been difficult to explain in earlier studies of copper amine oxidase raising questions concerning the mechanism of the oxidative half-reaction as well as the physical origins of the ¹⁸O KIEs.^{12,19,20} Here the isotope effects are interpreted in light of extensive density functional calculations using methods we have recently established by benchmarking calculated values against those experimentally determined for structurally-defined, synthetic copper-oxygen compounds.²¹ The difficulties encountered in earlier works are discussed and the ¹⁸O KIEs are shown to fall precisely within the computationally-derived limits. We believe that this combined experimental/computational approach, applied more commonly to organic reactivity,²² holds great promise for characterizing intermediates in metalloenzymes which activate O₂ as well as those which process reactive oxygen species (O₂•⁻ and H₂O₂) using redox metal cofactors.

Experimental

General

PSAO was isolated in 98% purity following a previously described method.²³ Specialty chemicals were obtained from Sigma in the highest purity available unless noted otherwise. Substrate stock solutions were prepared from putrescine (1,4-diaminobutane) in its free base or dihydrochloride form. Putrescine with all carbons deuterium-labeled (1,4-butane-d₈-diamine dihydrochloride and 1,4-butane-d₈-diamine) 99.5% and α,α-d₂-benzylamine 99% were purchased from C/D/N Isotopes. The percent protio contamination was confirmed to be between 0.4 and 0.6% by ¹H NMR.

A. Spectrophotometric measurements

Spectrophotometry was performed using an 8452 or 8453 diode array system (Agilent), a Cary 6000i (Varian) or a RSM1000 stopped-flow (OLIS). Optical spectra were recorded under a rigorously anaerobic atmosphere at 25 °C unless noted otherwise. Conventional spectrophotometry was performed using re-sealable quartz cells (Starna). Stopped-flow measurements were performed inside a glovebox (MBraun). Enzyme solutions were degassed through multiple cycles of vacuum and nitrogen or vacuum and argon. Titration experiments were performed by adding substrates using a glovebox or standard Schlenk technique. The concentration of oxidized enzyme, containing two quinocofactors per mole of protein, was determined from the absorbance due to TPQ_{ox}. The TPQ_{ox} has an extinction coefficient of $\epsilon_{495\text{nm}} = 2,450 \text{ M}^{-1}\text{cm}^{-1}$ (per monomer) at pH 7.2.²³ On this basis, the extinction coefficient of the semiquinone form of the enzyme was determined to be $\epsilon_{465\text{nm}} = 7,000 \text{ M}^{-1} \text{ cm}^{-1}$ (per monomer).²⁴

B. Steady-State Kinetics

Measurements of initial O₂ consumption rates at steady-state were performed using a Clark-type oxygen electrode (Yellow Springs Inc.; 5300A voltmeter and 5331A probe). The ionic strength was maintained at $0.1 \pm 0.02 \text{ M}$ at varying pH and temperature. Chloride was introduced as a counterion for the protonated amine substrate in some experiments with no discernible effect. It was, thus, confirmed that Cl[−] does not inhibit putrescine oxidation or O₂ reduction by PSAO.²⁵

A standard assay was developed to check the enzyme concentrations. An air-saturated solution containing $\sim 272 \text{ } \mu\text{M}$ O₂ and 5 mM putrescine at pH 7.2 was used, where $v/[E]_{\text{T}}$ (22 °C) = 197 s^{-1} per dimer, i.e. 98.5 s^{-1} per monomer. This assay agreed with the protein concentration determined from the absorbance of TPQ_{ox} at 495 nm as well as its absorbance after titration with phenylhydrazine. Phenylhydrazine titrations indicated the presence of 1.6–2.0 equivalents of TPQ per dimer in all batches of protein. The concentration of active enzyme was additionally checked by comparison to the established specific activity with benzylamine.²³ Initial rates were confirmed to vary, as expected, in proportion to the enzyme concentration. Change in enzyme activity at the extremes of pH and temperature was monitored by pre-incubating stock solutions (1–10 minutes) under the relevant conditions followed by a standard assay.

Kinetic data were collected between 5 and 50 °C using the O₂ electrode in a water jacketed reaction chamber equipped with a re-circulating bath (VWR 116-0S). Reaction solutions were typically preequilibrated for several minutes against varying mixtures of O₂ and N₂ at 1 atm prior to initiating the reaction by addition of the enzyme (2.5–80 nM). Initial rates of O₂ uptake exceeded the electrode's background drift rate by at least a factor of ten. The enzymatic rate was calculated from the most linear portion of the decay curve approximately ten seconds after mixing of the enzyme and substrate solution.

Initial rate data at varying substrate concentrations were analyzed using Kaleidagraph 4.0 (Synergy Software). Kinetic parameters were obtained by fitting at least ten points to the Michaelis-Menten expression (Eq 3); v is the initial rate, $[E]_{\text{T}}$ is the total active enzyme concentration, $^{\text{ap}}K_{\text{M}}$ is the apparent Michaelis constant and $^{\text{ap}}k_{\text{cat}}$ is the apparent rate constant for enzyme turnover. The limiting k_{cat} , K_{M} and $k_{\text{cat}}/K_{\text{M}}$ values are reported with errors of $\pm 2\sigma$ derived from the non-linear curve-fitting analysis.

$$\frac{v}{[E]_{\text{T}}} = \frac{^{\text{ap}}k_{\text{cat}} [S]}{^{\text{ap}}K_{\text{M}} + [S]} \quad (3)$$

1. Kinetics at Varying pH—The following buffers were used to study the kinetics at varying pH: 0.1000 M MES (2-(*N*-morpholino)ethane sulfonic acid) at pH 5.2, 0.0850 M sodium

phosphate at pH 6, 0.0500 M sodium phosphate at pH 7.2, 0.0160 M sodium pyrophosphate at pH 8, 0.0136 M sodium pyrophosphate at pH 9, 0.0107 M sodium pyrophosphate at pH 10. The ionic strength was maintained at 0.1 ± 0.02 M by varying the buffer concentration. The absence of specific buffer effects was confirmed by comparing $k_{\text{cat}}/K_{\text{M}}(\text{O}_2)$ in two different buffers at the same pH and ionic strength; for example, MES and phosphate buffer at pH 6.2.

2. Solvent Isotope Effect Studies—Deuterated buffer solutions were prepared as outlined above using salts enriched by dissolution in D_2O (99.9 % Cambridge Isotope Laboratories) and evaporation to dryness. Solution pH and pD values ($\text{pD} = \text{pH}_{\text{reading}} + 0.4$) were determined using an Accumet Research pH meter at 22 °C. Small corrections of -0.0028 unit/°C (phosphate) and 0.01 unit/°C (pyrophosphate) were applied above and below room temperature. Solvent isotope effects are reported as the average of at least three measurements with the errors propagated according to Eq 4; $k_{\text{H}} = [k_{\text{cat}}/K_{\text{M}}(\text{O}_2)]_{\text{H}_2\text{O}}$, $k_{\text{D}} = [k_{\text{cat}}/K_{\text{M}}(\text{O}_2)]_{\text{D}_2\text{O}}$ and $\Delta k_{\text{H or D}}$ corresponds to the standard error from the non-linear regression analysis.

$$\Delta \left(\frac{k_{\text{H}}}{k_{\text{D}}} \right) = \sqrt{\left(\frac{1}{k_{\text{D}}} \right)^2 (\Delta k_{\text{H}})^2 + \left[\frac{-k_{\text{H}}}{(k_{\text{D}})^2} \right]^2 (\Delta k_{\text{D}})^2} \quad (4)$$

3. Substrate Deuterium Kinetic Isotope Effect Studies—Deuterium kinetic isotope effects were measured by comparing rates obtained with d_8 -putrescine and $\alpha, \alpha\text{-d}_2$ -benzylamine with those of the corresponding per-protio substrates. Errors were propagated as described above; in Eq 4, k_{H} and k_{D} for the protio and deutero substrates, respectively, are associated with either k_{cat} or $k_{\text{cat}}/K_{\text{M}}$. The uncompetitively determined kinetic isotope effects are reported conservatively with errors of $\pm 2\sigma$.

4. Viscosity Effects—Experiments to probe contributions from substrate diffusion to $k_{\text{cat}}/K_{\text{M}}$ were conducted using sucrose or glycerol as the solvent viscosogen. Solution viscosities were determined relative to a solution of buffer using an Ostwald viscometer at 22 °C. Data were analyzed per the relationship: $[k_{\text{cat}}/K_{\text{M}}(\text{O}_2)]^0/[k_{\text{cat}}/K_{\text{M}}(\text{O}_2)] = (\eta/\eta^0)^{\text{exp}}$; the “0” designates the absence of viscosogen. According to the Stokes-Einstein relation, an exponent of 1 should be observed for diffusion-limited binding of the amine substrate or diffusion-limited dissociation of the aldehyde product.²⁶ A smaller, empirically-determined exponent of 0.5 has been proposed to describe deviations from Stokes-Einstein behavior for small diatomic solutes like O_2 .²⁷

C. Competitive Oxygen Kinetic Isotope Effects

Oxygen kinetic isotope effects (^{18}O KIEs) were determined using a previously described competitive technique and a home-built high vacuum apparatus.²⁸ Natural abundance O_2 was used in these experiments. Analysis performed by isotope ratio mass spectrometry (IRMS) afforded the $^{18}\text{O}/^{16}\text{O}$ content of CO_2 samples, which were prepared by quantitatively combusting the unreacted O_2 isolated from solutions before and after introducing PSAO.

^{18}O KIE measurements were performed over a range of temperatures (at 5, 22 or 47 °C) in sodium phosphate buffer (pH 7.2, $\mu = 0.1$ M). In these experiments, putrescine-containing solutions were saturated with O_2 or He/O_2 mixtures and then loaded into an injectable glass reaction chamber. The chamber was equipped with a movable piston and two-way crossover stopcock for sampling the solution. Connection of the chamber to the vacuum apparatus allowed fixed volumes of the reaction solution (typically 10 mL) to be withdrawn *in vacuo* at varying stages of reaction. No O_2 consumption was detectable when putrescine-containing solutions were allowed to stand for 1-3 hours in the absence of enzyme. Reactions were initiated by injecting a solution of PSAO through a re-sealable septum. The enzymatic reaction was quenched prior to removing the O_2 by addition of 5-sulfosalicylic acid (20 mg) in 0.5 mL 85%

H₃PO₄. Samples were prepared after isolating the O₂ from other condensable gases. The O₂ was quantitatively converted to CO₂ by combustion over graphite with platinum wire at 900 °C. CO₂ samples were condensed into dry glass tubes and flame sealed after determining the pressure of gas using a capacitance manometer (Omega PX238). The precision of the pressure measurements was typically ± 3 % with the CO₂ related to the fractional consumption of O₂ by the enzymatic reaction.

IRMS analysis of CO₂ samples was achieved using a dual-inlet, stable isotope ratio mass spectrometer in the Environmental Isotope Laboratory at the University of Waterloo (Ontario, Canada). The ¹⁸O/¹⁶O in samples prepared using the procedure outlined above was precise to ± 0.0003. The isotope fractionation of the unreacted O₂ was interpreted using Eq 5 which expresses the ¹⁸O KIE in terms of a ratio of ratios; i.e. the ¹⁸O/¹⁶O (*R_f*) at a specific fractional conversion (*f*) relative to the ¹⁸O/¹⁶O (*R₀*) prior to the enzymatic reaction. The ¹⁸O KIEs reported in this work were determined at fractional conversions from ca. 5 to 55 % by solving Eq 5. The KIE is quoted as the average of at least five independent measurements with errors quoted as ± 1σ about the mean.

$$^{18}\text{OKIE} = \left[1 + \frac{\ln(R_f/R_0)}{\ln(1-f)} \right]^{-1} \quad (5)$$

D. Density Functional Calculations

Calculations at the density functional level of theory (DFT) were performed using *Gaussian03W*.²⁹ Molecular geometries were optimized with the *mPWPW91* functional³⁰ and the following atomic orbital basis functions:³¹ CEP-31G for Cu,³² 6-311G* for N and O, 6-31G for C, and STO-3G for H. Complexes formally assigned as copper(II) end-on (η¹) superoxide species were assumed based on previous results²¹ to have triplet ground states. The end-on (hydro)peroxide or side-on (η²) peroxide species have doublet ground states. Calculations on these states were thus performed using unrestricted Kohn-Sham (KS) DFT.³³ The stability of KS self-consistent field solution was confirmed for each optimized structure. Molecular orbitals were visualized for all structures and the singly occupied molecular orbitals (SOMOs) confirmed to be associated with copper and/or dioxygen.

To match the active site structure of PSAO as well as compare structures with differing sterics and electronics about Cu^{II}, DFT calculations were performed with imidazole or methylimidazole as supporting ligands. In one set of calculations the methylimidazole was constrained to interact through the δ-imino rather than the ε-imino group, as seen in the published crystal structure of PSAO.¹⁵ Vibrational frequencies were calculated analytically for each optimized structure within the harmonic oscillator approximation.³³ All minima were characterized by real frequencies in all but a few cases where imaginary frequencies (from 4 to 9 cm⁻¹) with negligible isotope shifts were observed.

We recently established a density functional method to reproduce experimentally determined oxygen equilibrium isotope effects (¹⁸O EIEs).²¹ The latter study demonstrated the need for using full sets of stretching frequencies associated with the ¹⁶O–¹⁶O and ¹⁶O–¹⁸O isotopologues of the reactant and product states in the calculations. We follow this established computational method again using the Bigeleisen and Goeppert-Mayer formalism to calculate ¹⁸O EIEs.^{21,34} Certain calculations were performed on structures where O₂ binds to copper an asymmetric manner. We previously demonstrated that neglecting the small intramolecular isotope effect (ca. 2%), by assuming a 50/50 average of Cu¹⁶O–¹⁸O and Cu¹⁸O–¹⁶O structures, has an insignificant effect on the calculated ¹⁸O EIE.²¹

Studies of the ¹⁸O EIEs have indicated that the effects can exhibit significant variations with temperature depending on the population of isotopically sensitive low frequency modes.²¹

Therefore, in this study the temperature dependence of the ^{18}O EIEs was carefully evaluated for each of the calculated structures. In most cases it was determined that the ^{18}O EIEs at 22 °C were indistinguishable from the maximum ^{18}O EIE, which generally occurs at a lower temperature.

Results

A. The Identity of the Resting Reduced Enzyme

PSAO was reduced anaerobically to probe the equilibrium between the two states: $\text{E}(\text{Cu}^{\text{II}}, \text{TPQ}_{\text{red}})$ and $\text{E}(\text{Cu}^{\text{I}}, \text{TPQ}_{\text{sq}})$ (K_{int} in Figure 2). Experiments were performed by titrating the enzyme-containing solution with the substrate (putrescine, *N,N*-dimethylaminomethylbenzylamine or benzylamine) under an O_2 -free atmosphere. Conventional mixing and rapid-mixing techniques were employed to generate the same equilibrium mixture. K_{int} was determined from the absorbance due to the TPQ_{sq} and the initial TPQ_{ox} . The results were found to be independent of the protein preparation as well as the presence of excess amine.

The pH dependence of K_{int} was investigated at varying pH at 22 °C. The end-point was confirmed by the absence of spectral change upon addition of excess substrate or by addition of sodium cyanide (NaCN) which shifts the equilibrium to favor the enzyme-bound semiquinone, i.e. the $\text{E}(\text{Cu}^{\text{I}}, \text{TPQ}_{\text{sq}})$ state.^{13,35,36} The TPQ_{red} has an insignificant extinction coefficient between 450 and 500 nm,¹² therefore, its absorbance contribution was neglected. Titration of the protein with phenylhydrazine corroborated the results and indicated that all of the TPQ_{ox} was present in an amine-reactive form.

The optical spectra at varying pH report on the protonation states of the TPQ species in PSAO. The absorbance due to TPQ_{ox} blue shifts from 508 nm to 485 nm as the pH is raised from 6 to 10 most likely due to deprotonation of the hydroxyl group in the 2 or 4 position.³⁷ The absence of a pH-dependent variation in the TPQ_{sq} optical spectrum suggests that this species exists in its neutral form (Figure 3a). Since the optical bands at 434 and 465 nm arise from vibronic structure of the TPQ_{sq} ,³⁸ they would be expected to change upon protonation. The observed behavior is as expected on the basis of solution studies where the semiquinone radical cation of 4-aminoresorcinol exhibits a pK_a of 3.4.³⁹ Although unobservable in PSAO, partial deprotonation of TPQ_{red} and TPQ_{sq} would be expected at sufficiently high pH in view of model studies which revealed a pK_a of 9.59 for 6-amino-4-ethylresorcinol.³⁷

The spectrophotometric titration results indicate that K_{int} weakly depends upon the solution pH (Figure 3b). The fraction of $\text{E}(\text{Cu}^{\text{I}}, \text{TPQ}_{\text{sq}})$ increases approximately four-fold upon lowering the solution pH from 10 to 5. These results are opposite to those which would be expected to accompany protonation of the anionic or neutral TPQ_{red} where changing the pH by one unit should decrease the concentration of $\text{E}(\text{Cu}^{\text{I}}, \text{TPQ}_{\text{sq}})$ relative to $\text{E}(\text{Cu}^{\text{II}}, \text{TPQ}_{\text{red}})$ by a factor of 10 (1 log unit in K_{int}). The results can alternatively be explained by protonation of peripheral residues. Increasing the positive charge in the active site may increase the $\text{Cu}^{\text{II/I}}$ redox potential, favoring K_{int} . The titration results clearly show that, at physiological pH and 22 °C, the reduced enzyme exists largely (~80%) in the $\text{E}(\text{Cu}^{\text{I}}, \text{TPQ}_{\text{sq}})$ form. This result would impact the interpretation of the kinetic data if the reaction with O_2 were rate-determining.

B. Kinetics of the Oxidative Half-Reaction

1. pH and pD Profiles—The spectroscopic redox titration results are in marked contrast to the O_2 -dependent kinetics. We find that $k_{\text{cat}}/K_{\text{M}}(\text{O}_2)$ at 22 °C is unchanged between pH 6.0 and 9.5 (Figure 4b). The average $k_{\text{cat}}/K_{\text{M}}(\text{O}_2)$ in D_2O is slightly lower than in H_2O over the same pD range suggesting a small solvent kinetic isotope effect of 1.2 ± 0.2 . The effect is

consistent with a prototropic pre-equilibrium and the absence of rate-determining proton transfer from a solvent-exchangeable site.

Below pH 6 there is a precipitous fall-off in rate constant that is more pronounced in D₂O than in H₂O. The observed behavior is consistent with a protonation event that deactivates the enzyme. It is tempting to associate this event with formation of the cationic TPQ_{red} but a parallel change in the concentration of the E(Cu^I,TPQ_{sq}) is not seen in the spectrophotometric redox titrations at low pH. Instead, the concentration of E(Cu^I,TPQ_{sq}) increases monotonically to ~90%. The results indicate that the intrinsic pK_a values, such as those associated with a copper-bound water molecule or TPQ cofactor, cannot be discerned from the kinetics. Such behavior can occur when complex equilibria precede the irreversible step (*vide infra*).⁴⁰ At this stage, the only conclusion that can be drawn from the different pH profiles of $k_{\text{cat}}/K_{\text{M}}(\text{O}_2)$ and k_{cat} is that the two parameters do not share a common irreversible step.

2. Solvent Viscosity Studies—The dependence of $k_{\text{cat}}/K_{\text{M}}(\text{O}_2)$ upon solution viscosity was examined to address whether the bimolecular rate constant contains a step controlled by the diffusion of O₂. Experiments were performed at relative viscosities, η/η^0 from 4.1 to 5.1. Such high relative viscosities are needed to observe an effect in cases where small solutes like O₂ are involved and show deviations from ideal Stokes-Einstein behavior.²⁷ No sign of a viscosity effect was detectable at pH 7.2 and 22 °C indicating the absence of an encounter-controlled reaction. The $k_{\text{cat}}/K_{\text{M}}(\text{O}_2)$ determined in the presence of glycerol ($2.3 \pm 0.3 \times 10^6 \text{ M}^{-1}\text{s}^{-1}$) or sucrose ($2.5 \pm 0.2 \times 10^6 \text{ M}^{-1}\text{s}^{-1}$) is slightly increased from the $k_{\text{cat}}/K_{\text{M}}(\text{O}_2)$ in the absence of viscosogen ($2.1 \pm 0.2 \times 10^6 \text{ M}^{-1}\text{s}^{-1}$) suggesting small non-specific effects of the viscosogen on the protein structure. Such non-specific effects primarily impact k_{cat} which changes from $99 \pm 2 \text{ s}^{-1}$ in buffer-only solutions to 72 ± 2.5 in the presence of glycerol ($\eta/\eta^0 = 4.1\text{--}5.2$) and $147 \pm 20 \text{ s}^{-1}$ in the presence of sucrose ($\eta/\eta^0 = 4.5$). Control experiments revealed that $k_{\text{cat}}/K_{\text{M}}(\text{putrescine}) = 8.5 \pm 0.2 \times 10^5 \text{ M}^{-1}\text{s}^{-1}$ is characterized by a small positive viscosity effect upon addition of glycerol (slope of 0.20 ± 0.11) suggesting partial rate-limitation by substrate binding.

3. Oxygen Kinetic Isotope Effects—The ¹⁸O KIE corresponding to $[k_{\text{cat}}/K_{\text{M}}(^{16,18}\text{O}_2)]/[k_{\text{cat}}/K_{\text{M}}(^{16,16}\text{O}_2)]$ is readily determined using a competitive isotope fractionation technique and natural abundance O₂.²⁸ As outlined above, the reaction mixture is sampled at different stages to probe the changes in the ¹⁸O/¹⁶O as the reaction progresses. During PSAO catalysis, the heavier isotopologues accumulates in the unreacted O₂ due to the faster reaction of ¹⁶O–¹⁶O than ¹⁸O–¹⁶O and a normal ¹⁸O KIE is observed. Data obtained using different preparations of PSAO and amine co-substrates are shown fitted to isotope fractionation expression (Eq 5) to illustrate the precision of the competitive ¹⁸O KIE measurements (Figure 5).

Experiments at pH 7.2 indicate an ¹⁸O KIE = 1.0136 ± 0.0014 at 22 °C. The isotope effect is independent of the O₂ consumed, as expected for a reaction where the contribution of the isotopically sensitive step to $k_{\text{cat}}/K_{\text{M}}(\text{O}_2)$ remains unchanged. The ¹⁸O KIE is also independent of H₂O₂ accumulation during the reaction as indicated by the lack of effect upon adding horseradish peroxidase and a sacrificial reductant, either guaiacol or ferrocyanide, to scavenge the H₂O₂ from reaction solutions.

Importantly, the isotope fractionation experiments performed over a range of temperatures provide no evidence for kinetic complexity or a change in the step which limits $k_{\text{cat}}/K_{\text{M}}(\text{O}_2)$. The ¹⁸O KIE at pH 9 and 22 °C, 1.0122 ± 0.0020 , is the same within experimental error of that quoted above for pH 7.2. In addition the pH 7.2 data are independent of temperature falling within the narrow range of 1.0133 ± 0.0017 at 5 °C and 1.0140 ± 0.0010 at 47°C. These results which exclude kinetic complexity allow rigorous analysis of the ¹⁸O KIEs using DFT methods.

In addition the temperature invariant ^{18}O KIEs support the interpretation of activation parameters determined for $k_{\text{cat}}/K_{\text{M}}(\text{O}_2)$ over the same range.

C. Deuterium Kinetic Isotope Effects on Amine Oxidation

Substrate deuterium kinetic isotope effects were determined to assess the contribution from C–H cleavage to k_{cat} and, consequently, the relative extents to which the oxidative and reductive half-reactions limit enzyme turnover. Uncompetitive deuterium KIEs ($^{\text{D}}k_{\text{cat}}$ and $^{\text{D}}k_{\text{cat}}/K_{\text{M}}$) were analyzed with putrescine and benzylamine; these fast and slow substrates exhibit rate constants that vary by more than 10^2 at pH 7.2 and 22 °C. In experiments at saturating levels of O_2 , partially rate-limiting C–H cleavage was indicated for both substrates: $^{\text{D}}k_{\text{cat}}(\text{putrescine}) = 4.1 \pm 0.2$ and $^{\text{D}}k_{\text{cat}}/K_{\text{M}}(\text{putrescine}) = 3.3 \pm 0.6$ and benzylamine: $^{\text{D}}k_{\text{cat}}(\text{benzylamine}) = 2.3 \pm 0.2$ and $^{\text{D}}k_{\text{cat}}/K_{\text{M}}(\text{benzylamine}) = 9.5 \pm 1.6$.

Differences in the extent to which C–H cleavage is rate-limiting were further observed upon varying the pH. The range of $^{\text{D}}k_{\text{cat}}$ for putrescine was 4.2 ± 0.4 at pH 8 and 3.4 ± 0.2 at pH 10. In contrast, $^{\text{D}}k_{\text{cat}}/K_{\text{M}}(\text{putrescine})$ decreased dramatically from 9.2 ± 1.0 to 1.1 ± 0.4 as the pH was varied from 6 to 10. These results are consistent with a common irreversible step in k_{cat} and $k_{\text{cat}}/K_{\text{M}}(\text{putrescine})$ changing from one dominated by C–H deprotonation to one dominated by formation of the substrate Schiff-base.

The temperature dependence of the deuterium KIE upon putrescine oxidation was examined at pH 7.2 under the same conditions used to determine the activation parameters for k_{cat} and $k_{\text{cat}}/K_{\text{M}}(\text{O}_2)$. The $^{\text{D}}k_{\text{cat}}$ increased from 3.3 ± 0.2 at 5 °C to 5.1 ± 0.2 at 47 °C. These values are significantly below the intrinsic isotope effect, which is estimated to be ~ 9.2 on the basis of the above-mentioned measurements at low pH. The trend with temperature is opposite that expected for a primary kinetic isotope effect determined largely by the influence of zero point energy on the activation barrier.⁴¹ Instead the variation in $^{\text{D}}k_{\text{cat}}$ arises from an increase in the extent to which C–H cleavage is rate-limiting at high temperatures. Thus, k_{cat} consists of multiple steps with C–H cleavage contributing by ~ 35 to 55%. The dissociation of the product aldehyde and the release of H_2O_2 are also possible contributors to this kinetic parameter.

D. The pH/pD Dependence of $k_{\text{cat}}(\text{putrescine})$

The pH and pD profiles of $k_{\text{cat}}(\text{putrescine})$ resemble those previously published for other eukaryotic amine oxidases and substrates.^{42–44} We find the limiting rate constants obtained from experiments at varying amine or O_2 to be poorly fitted by two and three pK_{a} models. This observation is not surprising since $k_{\text{cat}}(\text{putrescine})$ is a kinetically complex parameter, as demonstrated by the evaluation of $^{\text{D}}k_{\text{cat}}$ as a function of pH and temperature. The pH dependence of k_{cat} is less complex in the low pH regime where apparent pK_{a} values of 5.2 (H_2O) and 6.0 (D_2O) are observed together with a variation of one order of magnitude in rate per pH unit. This behavior is consistent with ionization of the active site Asp within the substrate Schiff-base complex.¹² In the basic regime, k_{cat} in H_2O and D_2O are indistinguishable within the limits of error. Control experiments indicate that the diminished rate constant does not arise from irreversible denaturation of the protein suggesting the presence of a high pH form of the enzyme with lower overall activity.

E. Thermal Activation Parameters

Steady-state kinetic parameters were evaluated at pH 7.2 at several temperatures between 5 and 50 °C (Figure 6). In spite of the kinetic complexity, the temperature dependence of k_{cat} (Figure 6b) is characterized by moderate scatter in the data and a relatively linear Arrhenius plot with $E_{\text{act}} = 10.5 \pm 1.2 \text{ kcal mol}^{-1}$ and $A = (5.7 \pm 3.9) \times 10^9 \text{ s}^{-1}$. The $\Delta H^{\ddagger} = 9.9 \pm 1.1 \text{ kcal mol}^{-1}$ and $\Delta S^{\ddagger} = -14.8 \pm 2 \text{ e.u.}$ are obtained by assuming a pre-exponential frequency factor

of 10^{13} s^{-1} . These activation parameters reflect multiple unimolecular steps including C–H deprotonation.

The Arrhenius plot of $k_{\text{cat}}/K_{\text{M}}(\text{O}_2)$ versus temperature (Figure 6a) is also linear with $E_{\text{act}} = 12.0 \pm 1.1 \text{ kcal mol}^{-1}$. A surprisingly large Y-intercept indicates a pre-exponential term of $A = (1.4 \pm 1.5) \times 10^{15} \text{ M}^{-1}\text{s}^{-1}$. Assuming an adiabatic pre-exponential frequency factor of $10^{11} \text{ M}^{-1}\text{s}^{-1}$,⁴⁵ the activation parameters are $\Delta H^\ddagger = 11.4 \pm 1.0 \text{ kcal mol}^{-1}$ and $\Delta S^\ddagger = 19 \pm 3 \text{ e.u.}$ The observed *positive activation entropy* is inconsistent with a simple bimolecular reaction of O_2 , corroborating the proposal, to explain the pH-dependent redox titration and pH independent kinetics, that $k_{\text{cat}}/K_{\text{M}}(\text{O}_2)$ reflects a multi-step mechanism.

F. Steady-State Intermediates

Reactions in the presence of saturating O_2 and amine were monitored spectrophotometrically to determine which intermediates accumulate in the steady-state. Experiments were first performed with benzylamine which exhibits $k_{\text{cat}} = 0.75 \text{ s}^{-1}$, $K_{\text{M}}(\text{benzylamine}) = 322 \pm 67 \text{ }\mu\text{M}$ and $K_{\text{M}}(\text{O}_2) \sim 370 \text{ nM}$. The $K_{\text{M}}(\text{O}_2)$, although too low to be measurable using an O_2 electrode, was calculated from the $k_{\text{cat}}/K_{\text{M}}(\text{O}_2) = (2.1 \pm 0.2) \times 10^6 \text{ M}^{-1}\text{s}^{-1}$ (per monomer) determined with putrescine at 22°C and pH 7.2 ($\mu = 0.1 \text{ M}$). Due to the slow turnover rate, the approach to steady-state could easily be monitored with this substrate using a conventional UV-Vis spectrophotometer at 20°C (Figure 7).

The data in Figure 7 were obtained by introducing the enzyme ($8.5 \text{ }\mu\text{M}$ PSAO, $17 \text{ }\mu\text{M}$ TPQ_{ox}) into an air saturated solution ($284 \text{ }\mu\text{M}$ O_2) containing 3.85 mM benzylamine. Upon mixing, the TPQ_{ox} rapidly converts to a species with a broad absorbance centered at 460 nm ; this species is assigned as the product Schiff-base on the basis of previous stopped-flow kinetic studies.⁴⁶ The absorbance is unchanged as the enzyme continues to turnover (1-16 seconds) at saturating levels of both substrates. Notably, there is no evidence of TPQ_{sq} accumulation in this steady-state mixture, indicating no contribution from an ET step in the oxidative half-reaction. The TPQ_{sq} eventually appears (17-21 seconds) approaching its expected concentration of $\sim 14 \text{ }\mu\text{M}$ as the O_2 is depleted below $K_{\text{M}}(\text{O}_2)$.

The observation of the steady-state is more challenging with putrescine because of the elevated kinetic parameters. Values (per monomer) at 22°C are: $k_{\text{cat}} = 91.5 \pm 4.8 \text{ s}^{-1}$, $K_{\text{M}}(\text{putrescine}) = 140 \pm 10 \text{ }\mu\text{M}$, $K_{\text{M}}(\text{O}_2) = 44.6 \pm 4.2 \text{ }\mu\text{M}$, values for each substrate. Experiments required the use of a stopped-flow spectrophotometer for rapid mixing and observation of the reaction solution. The results obtained upon mixing an O_2 -saturated solution of PSAO ($20 \text{ }\mu\text{M}$, $40 \text{ }\mu\text{M}$ TPQ_{ox}) with an O_2 -saturated solution of putrescine (10 mM) at pH 7.2 and 24°C are shown in Figure 8. The final concentrations of enzyme and putrescine in the observation cell are one half of those quoted above, while the O_2 concentration is maintained at $\sim 1 \text{ mM}$.

Monitoring optical changes between $352\text{--}577 \text{ nm}$ over 1 second indicated the steady-state was attained in the time of mixing and lasted for ~ 250 milliseconds. Between 250 and 320 ms a rapid change gave rise to the spectrum characteristic of the reduced enzyme ($10 \text{ }\mu\text{M}$ PSAO) containing $\sim 80\%$ $\text{E}(\text{Cu}^{\text{I}}, \text{TPQ}_{\text{sq}})$. Global analysis was used to obtain the initial, steady-state mixture (red) and final, E_{red} (yellow) spectra. In the initial spectrum, the sloping absorbance with $\lambda_{\text{max}} = 340 \text{ nm}$ is consistent with the substrate Schiff base⁴⁷ while a small but significant absorbance at 500 nm indicates the presence of E_{ox} consistent with partially rate-limiting NH_3 dissociation. The λ_{max} at 340 nm has also been associated with iminoquinone, TPQ_{im} ,⁴⁸ which would buildup if hydrolysis to form NH_3 and/or H_2O_2 were rate-limiting. In view of the substrate deuterium KIE and the significant solvent isotope effect of 1.7 ± 0.1 upon k_{cat} at pH 7.2, up to 65% of this steady-state parameter may be limited by hydrolysis with the remaining contribution from C–H deprotonation resulting in accumulation of the optically indistinguishable substrate Schiff-base.

Discussion

Distinguishing inner-sphere from outer-sphere electron transfer (ET) reactions of oxygen is a fundamental problem in fields as diverse as biological and inorganic chemistry.^{5a,8} The ET mechanisms relate to the origins of catalytic O₂ reduction rates as well as the strategies used by enzymes to avoid oxidative damage by reactive oxygen species.⁴⁹ The role of the copper ion during catalysis by copper amine oxidases is a prime example.^{19,25,36} Inner-sphere electron transfer, where O₂ binds directly to the Cu^I, was originally assumed based on the observation that a significant fraction of the reduced enzyme existed in the E(Cu^I, TPQ_{sq}) state.^{13,17,50} Though the expected [Cu^{II}(η¹-O₂^{-I})]⁺ intermediate has eluded spectroscopic detection, another species assigned as a Cu^{II}(η²-O₂^{-II}) presumably with the accompanying TPQ_{im} has been observed by cryogenic x-ray crystallography studies of the *E. coli* amine oxidase.¹⁴ In the absence of correlations to the enzyme kinetics it is unclear if and how this intermediate may be involved in catalysis.

Numerous studies undertaken with the yeast enzyme HPAO have been interpreted in the context of an outer-sphere ET mechanism, where the electron transfers from E(Cu^{II}, TPQ_{red}) to O₂ pre-bound in a hydrophobic protein pocket.^{36,42,44,48,51} The binding step is evidenced by saturation behavior in the O₂-dependent kinetics of the single turnover reaction.⁴⁸ The most compelling support for outer-sphere ET comes from the observation that cobalt(II)-reconstituted HPAO catalyzes turnover at rates that approach those of the wild-type enzyme, although $k_{\text{cat}}/K_{\text{M}}(\text{O}_2)$ is significantly depressed. It has further been argued that the reconstituted HPAO exists exclusively in the Co^{II} state during catalysis. This observation is somewhat surprising in light of the spontaneous nature of reactions between amine-bound Co^{II} and O₂ which form Co^{III} in aqueous solution.⁵² Presumably the protein environment dramatically alters the Co^{III/II} redox potential and, thus, the reactivity of Co^{II} towards O₂. Although an ¹⁸O KIE has been reported for Co-HPAO, the large error in the measurement precludes its interpretation.

Stopped-flow analysis of the single-turnover reaction in wild-type HPAO points toward the first electron transfer in oxidative half-reaction as contributing roughly 30% to k_{cat} .⁴⁸ This is in marked contrast to the results presented here for PSAO, which demonstrate that k_{cat} and $k_{\text{cat}}/K_{\text{M}}(\text{O}_2)$ do not share a common step. Although there is no spectral evidence, rapid pre-equilibrium to form a high energy E(CuO₂, TPQ_{sq}) intermediate cannot rigorously be excluded based on the HPAO single-turnover kinetics. Spectroscopic observation of such copper superoxide intermediates is often difficult due to the unfavorable ΔS° associated with O₂-coordination. Kinetic methods, such as the oxygen isotope fractionation described here, are therefore needed to detect such species and to assess their involvement in catalysis.^{5,19,20,49}

A critical issue which has not been understood in studies of HPAO and bovine serum amine oxidase (BSAO) concerns the magnitude of the competitive ¹⁸O KIE.^{28a} The observations of small ¹⁸O KIEs of ~1.01 are difficult to reconcile with the much larger ¹⁸O KIEs of 1.025-1.030 expected for outer-sphere ET.^{19,28a,36,53} In earlier studies,^{42,44} an electrostatic interaction between Cu^{II} and the incipient O₂⁻ was proposed to cause diminution of the ¹⁸O KIE. For this to be true, the transition state must experience a change in force field which increases the net isotope shift of vibrational frequencies, $\Sigma(^{16,16}_{\text{v}} - ^{16,18}_{\text{v}})$, relative to the reactant O₂. This explanation presumes a bonding interaction in the transition state and, in turn, contradicts the formal definition of outer-sphere ET.⁴⁵ More recently attention has turned to the possibility that kinetic complexity is responsible for the smaller than expected ¹⁸O KIEs in HPAO and BSAO.^{19,36} In this work, we present evidence to the contrary, that ¹⁸O KIEs of ~1.01 are actually expected upon pre-equilibrium binding of O₂ to Cu^I.

I. The Internal Redox Equilibrium in PSAO

In PSAO the internal redox equilibrium occurs rapidly at physiological pH generating ~80% of the enzyme in the $E(\text{Cu}^{\text{I}}, \text{TPQ}_{\text{sq}})$ state on a timescale compatible with this species' involvement in enzyme catalysis. A similar amount of $E(\text{Cu}^{\text{I}}, \text{TPQ}_{\text{sq}})$ (~70%) is observed in the amine oxidase from lentil seedling (LSAO).^{24,50} In contrast, the $E(\text{Cu}^{\text{II}}, \text{TPQ}_{\text{red}})$ state dominates, making up less than 20% of the total reduced enzyme at physiological pH, in HPAO,³⁶ BSAO⁴⁴ and the bacterial enzyme from *Arthrobacter Globiformis*⁵⁴ (AGAO). Clearly there are differences in the protein active site structures which either promote or inhibit proton-coupled electron transfer and, hence, the equilibration of $E(\text{Cu}^{\text{II}}, \text{TPQ}_{\text{red}})$ and $E(\text{Cu}^{\text{I}}, \text{TPQ}_{\text{sq}})$ (Figure 2). The redox potential of the copper ion is likely to be a key factor as it is easily tuned by the protonation state of a bound water molecule.

The weak pH dependence of K_{int} in PSAO possibly reflects stabilization of $\text{Cu}^{\text{II}}\text{-OH}_2$, which is more oxidizing toward TPQ_{red} than $\text{Cu}^{\text{II}}\text{-OH}$. The slope of the log K_{int} versus pH plot is 0.27 is, however, inconsistent with a simple protonation/deprotonation event. Instead the effect of peripheral residues on either the E° or $\text{p}K_{\text{a}}$ of $\text{Cu}^{\text{II}}\text{-OH}_2$ is implied. More importantly, from pH 6-10 the concentration of $E(\text{Cu}^{\text{I}}, \text{TPQ}_{\text{sq}})$ varies by a factor of three while $k_{\text{cat}}/K_{\text{M}}(\text{O}_2)$ remains unchanged. A minimal change of a factor of 2.4 would be expected if O_2 were to bind to E_{red} in the rate-determining step⁵⁵. At very low pH the divergence is magnified by a further increase in $E(\text{Cu}^{\text{I}}, \text{TPQ}_{\text{sq}})$ concentration at the same time $k_{\text{cat}}/K_{\text{M}}(\text{O}_2)$ decreases by a factor of ~2. The lack of correlation between the position of the internal redox equilibrium and the steady-state rate constant is most readily attributed to a multi-step mechanism with the rate-determining step occurring only after the reversible binding of O_2 .

The electrostatic field which determines K_{int} was expected to be influenced by an active site lysine (Lys296), a residue that is conserved among the plant enzymes.¹⁵ Recent crystallographic studies under high pressures of xenon have suggested the possibility that the Lys is involved in of a conformationally-gated redox process where TPQ_{sq} is generated upon oxidative deamination of the side-chain.^{56,57} In this study we find no significant role for Lys296 in catalyzing the oxidative half-reaction; the $k_{\text{cat}}/K_{\text{M}}(\text{O}_2)$ in PSAO falls within an order of magnitude of the rate constants determined for HPAO⁴², BSAO⁴⁴ and AGAO,²⁵ all of which lack the active site Lys.

II. Interpretation of the Steady-State Kinetics

A. Intermediates during Enzyme Turnover—Spectrophotometrically examining the TPQ-derived species that accumulate in the steady-state affirmed the absence of a common irreversible step in $k_{\text{cat}}/K_{\text{M}}(\text{O}_2)$ and k_{cat} . Analysis of benzylamine oxidation revealed a small contribution from C–H deprotonation based on the deuterium substrate KIEs⁵⁸ and large accumulation of the product Schiff-base at 460 nm, consistent with the release of benzaldehyde limiting k_{cat} . The aldehyde must be released prior to the internal proton-coupled electron transfer, which is needed to prime the enzyme for reaction with O_2 in the proposed inner-sphere mechanism. Importantly, the prominent absorbance features due to the TPQ_{sq} are absent indicating that neither the first nor second ET step in the oxidative half-reaction contributes to k_{cat} with benzylamine.

The steps which control k_{cat} for putrescine oxidation are different from benzylamine, as expected due to the 10^2 difference in rate constants. Examination of $^{\text{D}}k_{\text{cat}}$ and $^{\text{D}}k_{\text{cat}}/K_{\text{M}}$ at varying pH and temperature indicates a significant contribution from C–H oxidation. The accumulation of the enzyme bound substrate Schiff-base complex, $E_{\text{ox}}\text{S}$, at 340 nm in the UV-Vis spectrum is, therefore, expected. The optical spectrum of the steady-state reaction mixture obtained from global analysis of the stopped-flow data within the first 250 ms bears out this expectation. In addition, the optical density around 500 nm suggests that the spectrum contains

some E_{ox} consistent with a contribution from NH_3 dissociation from the TPQ_{im} in the rate-determining step. Again, the spectral features due to TPQ_{sq} are absent indicating no rate limitation from ET steps in the oxidative half-reaction which occur prior to the release of H_2O_2 . The limit of detection is probably 0.02 absorbance units corresponding to 2.9 μM TPQ_{sq} .

B. The Oxidative Half-Reaction

1. Activation Parameters: The kinetic parameter $k_{cat}/K_M(O_2)$ does not share a common step with k_{cat} yet the temperature dependences are similarly large. The activation parameters determined in the adiabatic limit⁴⁵ for $k_{cat}/K_M(O_2)$ are: $\Delta H^\ddagger = 11.4 \pm 1.0$ kcal mol⁻¹ and $\Delta S^\ddagger = 19 \pm 3$ e.u. The positive entropy of activation argues against a simple bimolecular reaction of E_{red} and O_2 . This conclusion echoes that drawn on the basis of the pH dependence of K_{int} and its lack of correlation to $k_{cat}/K_M(O_2)$. The results implicate a multi-step process, where ET follows the entropically favored pre-binding of O_2 .

A common explanation for positive activation entropy in enzymes is the release of structured water from the protein active site.⁵⁹ Crystallographic studies reveal two water molecules bound to the Cu^{II} in the E_{ox} state of the copper amine oxidases (Figure 1).^{15,16} Release of water is expected upon reduction of Cu^{II} to Cu^I ; this reaction is suggested by XAS studies of dithionite-reduced PSAO which revealed a three-coordinate Cu^I center.⁶⁰ The dissociation of water upon reduction of Cu^{II} might be a general strategy used by copper-containing proteins to bind O_2 with moderate affinity. The PSAO reaction clearly proceeds with more favorable entropy than seen in related small molecule models. In particular, studies of synthetic copper or cobalt compounds which bind O_2 in an end-on manner are generally characterized by large negative entropy terms.^{21,61} Such behavior has also been proposed in O_2 -carrier proteins like myoglobin, where O_2 association with the metal center is significantly more favorable than in solution.⁶²

An alternative explanation for the positive ΔS^\ddagger in PSAO is that water release occurs upon binding of O_2 to an off-copper, hydrophobic pocket in the protein. In HPAO and BSAO, the partitioning of O_2 into a non-metal site forms the basis of the argument in favor of rate-determining outer-sphere ET,^{36,42,44} explaining why the wild type and cobalt enzymes exhibit similar values of k_{cat} . Though this phenomenon of O_2 "binding" in hydrophobic protein pockets is not well-understood it derives support from mutagenesis studies of HPAO⁶³ and more broadly from NMR⁶⁴ and x-ray crystallography under high pressures of xenon.^{10,56,57} Additional support comes from studies which reveal the collection of CO at non-metal sites in heme proteins responsible for gas transport.⁶⁵ The affinity of these sites for a diatomic gas molecule has been difficult to address, however.

2. Viscosity Studies: In earlier studies of BSAO⁴⁴ and HPAO⁴², viscosity effects were used to assess the extent to which diffusion of O_2 contributes to $k_{cat}/K_M(O_2)$. Very high viscosogen concentrations are required in these experiments due to the small size of O_2 and resulting deviations from Stokes-Einstein behavior.^{27,66} In the present study, solutions of high relative viscosity were employed yet none revealed an effect that could be construed as a diffusion-controlled reaction.

The absence of a viscosity effect upon $k_{cat}/K_M(O_2)$ does not, in itself, preclude the binding of O_2 to the enzyme in the rate-determining step. For small molecules in solution, these reactions are thermally activated not encounter-controlled. Typically, $\Delta G^\ddagger \gg 5$ kcal mol⁻¹ is observed as a result of significant ΔH^\ddagger and $-T\Delta S^\ddagger$ contributions. In support of the view that O_2 coordination requires overcoming a significant activation barrier, studies of competitive ^{18}O KIEs have revealed variations within the upper limit defined by the ^{18}O EIE and correlations to the size of ΔG^\ddagger .⁶⁷ This behavior is expected to be the same in metalloenzymes, allowing

changes in transition state structure upon binding of O₂ to be resolved by comparison of the ¹⁸O KIEs to the upper limit ¹⁸O EIEs for the O₂-adducts.

3. Oxygen Kinetic Isotope Effects: Some of the earliest isotope fractionation measurements were performed on copper amine oxidases.^{28a} The ¹⁸O KIE of 1.0097 ± 0.0010 determined for BSAO spanned a range of pH values and was proposed, on the basis of viscosity studies and the absence of significant TPQ_{sq} accumulation in the steady-state, to reflect outer-sphere ET.⁴⁴ The present work challenges the conclusions drawn for BSAO largely on the basis of the ¹⁸O KIE.

Recent studies have addressed the isotope effects upon outer-sphere ET to O₂. The major finding, both experimentally and computationally, is that the ¹⁸O KIEs range from 1.025-1.030 when the reaction is close to thermoneutral.^{19,28a,49a,53} The ¹⁸O KIEs are predicted to drop below 1.025 only when ΔG° becomes very favorable. To account for the low values seen for BSAO within the context of an outer-sphere ET mechanism, $\Delta G^\circ = -10 \text{ kcal mol}^{-1}$ would be required. Yet thermodynamic considerations detailed below indicate that ΔG° for ET from TPQ_{red} to O₂ should be highly unfavorable.

More recently, kinetic complexity in the O₂ reduction step has surfaced as a possible explanation of the small ¹⁸O KIEs seen for HPAO (1.0101 ± 0.0018) and possibly BSAO.¹⁹ An important result is provided by site-directed mutagenesis studies of HPAO in which an even smaller ¹⁸O KIE = 1.0074 ± 0.0008 was determined for the D630N mutant. Interestingly, D630N HPAO forms significantly more E(Cu^I, TPQ_{sq}) (36%) than the wild-type enzyme (15%) and exhibits a ten-fold increased $k_{\text{cat}}/K_M(\text{O}_2)$. Klinman and coworkers have maintained that the enzyme reacts by outer-sphere ET citing kinetic complexity as a possible origin of the suppressed ¹⁸O KIE.³⁶ Such complexity may arise from (i) a partially rate-limiting step prior to the first ET, such as O₂ “binding” to a non-metal site or (ii) a partially rate limiting step downstream of the first ET, such as the binding of the O₂^{•-} to Cu^{II}.

The ¹⁸O KIEs determined in this study for PSAO are only slightly larger than those seen in HPAO and BSAO yet temperature studies provide no indication of kinetic complexity. The ¹⁸O KIE = 1.0136 ± 0.0014 is unchanged from 5-47 °C. That changing the reaction temperature results in fortuitous cancellation of factors which cause the ¹⁸O KIE to be invariant seems very unlikely. Rather the ¹⁸O KIE determined for PSAO appears to reflect the intrinsic value, which we show in the following section using DFT methods, to be fully consistent with pre-equilibrium binding of O₂ to form [Cu^{II}(η^1 -O₂⁻)]⁺. Rate-determining ET from the TPQ_{sq} follows as indicated by analysis of the limiting ¹⁸O EIEs and the lack of evidence for proton transfer from the kinetic profiles in H₂O and D₂O.

4. Density Functional Calculations: The ¹⁸O EIEs calculated for potential intermediates in PSAO are presented in Table 1. The structures are arranged in order of decreasing O–O stretching frequency and increasing O–O bond length. All calculations were performed using the full sets of vibrational frequencies for the ¹⁶O–¹⁶O and ¹⁶O–¹⁸O isotopologues as we have previously described.^{21,34} Modeling the temperature dependence demonstrated that, in most cases, the magnitude of the calculated ¹⁸O EIE at 22 °C is indistinguishable from the maximum.³⁴ The influence of dielectric constant, which is exceedingly difficult to model in an enzyme active site,⁶⁶ was neglected since we previously observed that application of a polarized solvent continuum model can alter the stretching frequencies but only slightly affects the ¹⁸O EIE.²¹

The underlying assumption in using ¹⁸O equilibrium isotope effects (¹⁸O EIEs) as limiting values for ¹⁸O KIEs is that the change in bonding, or O₂ activation, in the transition state is more advanced than in the intermediate which precedes its formation. The trends seen in the

DFT calculations suggest that this should be the case in instances where the contribution from the reaction coordinate frequency can be neglected.⁶⁷

In order to have confidence in our computational modeling, we examined sixteen different structures manipulating the various factors which could impact the ^{18}O EIE. These factors include the addition of hydrogen-bonding interactions with water molecules, substituting the more electron rich methylimidazole for imidazole and constraining one methylimidazole ligand to interact through the more sterically encumbered δ -nitrogen, as seen in the published crystal structure of PSAO.¹⁵ The variables appeared to have little impact on the calculated ^{18}O EIEs, the primary determinant being the copper-oxygen bonds. This is not to say that the localized copper-oxygen modes could be used in isolation to give accurate assessment of the ^{18}O EIE. To the contrary, we have found that there is a significant contribution to the ^{18}O EIE from low frequency ligand modes which couple to the $\nu_{\text{O-O}}$, $\nu_{\text{Cu-O}}$ and $\delta_{\text{Cu-O-O}}$ vibrations.³⁴

C. Interpretation of the Oxygen Kinetic Isotope Effect—The ^{18}O KIEs determined for copper amine oxidases from different sources range from 1.0075 to 1.0136. The effects are close to the limits predicted for the formation of a superoxide, $[\text{Cu}^{\text{II}}(\eta^1\text{-O}_2^{-1})]^+$, intermediate. Entries 2-5 in Table 1 indicate a narrow range of values from 1.0092 to 1.0095 corresponding to this structure. When the ^{18}O KIE significantly exceeds 1.0095, as in PSAO, a pre-equilibrium binding of O_2 to reversibly form the $[\text{Cu}^{\text{II}}(\eta^1\text{-O}_2^{-1})]^+$ is indicated. In earlier work⁶⁷ we showed that in cases of irreversible O_2 binding the ^{18}O KIEs are depressed, approaching the ^{18}O EIEs only when kinetic barriers are very high $\Delta G^\ddagger \geq 15 \text{ kcal mol}^{-1}$. Rate-determining O_2 -binding may very well be the case in the D630N mutant of HPAO, where the ^{18}O KIE is less than the calculated ^{18}O EIE for the formation of the $[\text{Cu}^{\text{II}}(\eta^1\text{-O}_2^{-1})]^+$ intermediate.

A number of results point towards a multi-step process, with reversible O_2 binding in PSAO. These results include the absence of a viscosity effect, the positive entropy of activation determined in temperature studies, the lack of correlation between the position of K_{int} and $k_{\text{cat}}/K_{\text{M}}(\text{O}_2)$ as well as the favorable comparison of the ^{18}O KIE to the calculated ^{18}O EIE for the $[\text{Cu}^{\text{II}}(\eta^1\text{-O}_2^{-1})]^+$ structure. Therefore, the formation of a copper-peroxide intermediate in a single step is considered unlikely.

DFT calculations on the minimum energy end-on peroxide, $\text{Cu}^{\text{II}}(\eta^1\text{-O}_2^{-\text{II}})$, and side-on peroxide, $\text{Cu}^{\text{II}}(\eta^2\text{-O}_2^{-\text{II}})$, structures indicate large ^{18}O EIEs. Values of 1.017-1.024 and 1.027-1.031, respectively, mark the upper limits for the observed ^{18}O KIE. The variation within the calculated limiting ^{18}O EIEs for the end-on structure reflects the influence of hydrogen bonding to a water molecule (*cf.* entry 7 versus entries 6, 8 and 9). The smaller range seen for the side-on structure reflects (entries 11-14) reflects the insensitivity of the isotope effect to the steric and electronic changes which occur upon replacing imidazole with methylimidazole and forcing one ligand to coordinate through the δ -nitrogen.

Both peroxide structures are potential products of the rate-limiting step in PSAO, i.e. the ^{18}O KIE reflects all steps which contribute to $k_{\text{cat}}/K_{\text{M}}(\text{O}_2)$ beginning with O_2 encounter and leading up to the first irreversible (rate-determining) step. The end-on structure is favored over the side-on structure because the $\text{Cu}^{\text{II}}(\eta^2\text{-O}_2^{-\text{II}})$ represents a local minimum with its energy 2.3 to 4.8 kcal mol^{-1} greater than the $\text{Cu}^{\text{II}}(\eta^1\text{-O}_2^{-\text{II}})$. In order to keep both O nuclei coordinated to Cu^{II} in the side-on structure it was necessary to rotate the imidazole rings to a conformation where the higher energy geometry was accessible. It is interesting that coordination of dioxygen as a side-on peroxide ligand has been reported in a crystallographic study of *E. coli* amine oxidase,¹⁴ though it is unclear whether such an intermediate would form during catalysis in solution.

In the $\text{Cu}^{\text{II}}(\eta^1\text{-O}_2^{-\text{II}})$ proposed as the product of the rate-determining ET step in PSAO, the added electron appears significantly delocalized into the copper d-orbitals. Inspection of the singly occupied molecular orbital³⁴ together with the calculated $\nu_{\text{O-O}}$ and O–O bond distances in Table 1 indicate a continuum bonding description⁶⁸ where there is significant $\text{Cu}^{\text{I}}(\eta^1\text{-O}_2^{-1})$ character. This scenario changes when a proton is transferred to the terminal oxygen affording $[\text{Cu}^{\text{II}}(\eta^1\text{-O}_2^{-\text{II}}\text{H})]^+$. The absence of a significant solvent kinetic isotope effect upon $k_{\text{cat}}/K_{\text{M}}(\text{O}_2)$ in PSAO argues against the formation of the protonated peroxide species in the first irreversible step. In addition, the ^{18}O EIEs calculated for this structure (1.011-1.014, entries 15-18) are mostly too small to be consistent with the observed ^{18}O KIE.

III. An Inner-Sphere Mechanism of O_2 Reduction

The proposed O_2 reduction mechanism in PSAO involving reversible O_2 binding to Cu^{I} followed by ET from the TPQ_{sq} in the first irreversible step is shown in Scheme 1. The supporting evidence includes (i) the lack of correlation between $k_{\text{cat}}/K_{\text{M}}(\text{O}_2)$ and K_{int} , (ii) the positive ΔS^\ddagger derived from the temperature studies of $k_{\text{cat}}/K_{\text{M}}(\text{O}_2)$, (iii) the absence of rate-limitation by proton transfer, (iv) the absence of an encounter-controlled reaction of O_2 and (iv) the competitive ^{18}O KIE which is ostensibly free of kinetic complexity and lies between that calculated for the $[\text{Cu}^{\text{II}}(\eta^1\text{-O}_2^{-1})]^+$ and $\text{Cu}^{\text{II}}(\eta^1\text{-O}_2^{-\text{II}})$. The latter superoxide and peroxide structures are associated with Cu-O_2 and Cu-O_2^- , respectively, in Scheme 1.

In addition to accounting for the magnitude of ^{18}O KIE observed for copper amine oxidases, the mechanism in Scheme 1 might explain the lack of a correlation between the pH dependences of K_{int} and $k_{\text{cat}}/K_{\text{M}}(\text{O}_2)$. If O_2 were to act as a “sticky” substrate, the kinetically determined $\text{p}K_{\text{a}}$ values could be shifted outside of the experimental range. To understand this effect, the forward commitment to catalysis must be considered.⁴⁰ According to Scheme 1· Eq 6 is the rate expression for $k_{\text{cat}}/K_{\text{M}}(\text{O}_2)$.^{40b} Making the simplifying assumption that the rate constants for the initial ET steps are equal ($k_1=k_1'$), Eq 6 reduces to Eq 7. Eq 7 contains a term, $C_f=k_2/k_{-1}$ that corresponds to the internal forward commitment factor. The expression can be rewritten in terms of Eq 8 from which it is now obvious that when C_f is large, or O_2 is “sticky”, the measured $\text{p}K_{\text{a}}$ will be elevated from the intrinsic value. This behavior could explain the absence of a titratable residue in the pH profile of $k_{\text{cat}}/K_{\text{M}}(\text{O}_2)$ in PSAO. The observation of such a residue was anticipated on the basis of $\text{p}K_{\text{a}}$ values of ~ 9 determined for copper(II) bisaquo complexes,⁶⁹ which resemble the copper amine oxidase active site, as well as the $\text{p}K_{\text{a}}$ of 7.7 assigned to the $\text{Cu}^{\text{II}}\text{-OH}_2$ in HPAO.⁴²

$$k_{\text{cat}}/K_{\text{M}}(\text{O}_2) = \frac{k_2 \{k_1 + k_1' (K_{\text{a}} / [\text{H}^+])\}}{\{1 + (K_{\text{a}} / [\text{H}^+])\} \{k_2 + k_{-1} + (K_{\text{a}} k_1 k_{-1} / k_1' [\text{H}^+])\}} \quad (6)$$

$$k_{\text{cat}}/K_{\text{M}}(\text{O}_2) = \frac{k_2 k_1 / k_{-1}}{C_f + 1 + K_{\text{a}} / [\text{H}^+]} \quad (7)$$

$$\text{p}K_{\text{a}}(\text{intrinsic}) = \text{p}K_{\text{a}}(\text{measured}) - \log(1 + C_f) \quad (8)$$

IV. Catalysis of O_2 Reduction

A. Thermodynamic Considerations—The ability of copper amine oxidases to reduce O_2 to H_2O_2 is ultimately determined by the $2e^-$ redox potential of the reduced enzyme. The rate of the reaction can be understood in terms of the thermodynamics of the rate-determining step according to the tenets of Marcus theory.⁴⁵ We have previously shown that this is a useful formalism for understanding catalysis of ET as well as the propensity of an enzyme to react by an inner-sphere or outer-sphere pathway.^{48a,53,66}

Concentrating first on the feasibility of outer-sphere ET in copper amine oxidase, the thermodynamic driving force, ΔG° , is defined by the one-electron redox potentials of

TPQ_{red} and O₂. The ΔG° can be accessed using a thermodynamic cycle for TPQ_{red} following the method of Bordwell.⁷⁰

As a starting point, solution bond dissociation free energies are related to E° and pK_a values through Scheme 2. The relationship employs a thermodynamic constant $C = 57 \text{ kcal mol}^{-1}$ which reflects the formation and solubilization of the H• in aqueous solution.⁷¹ This type of analysis has been used widely to evaluate the bond dissociation free energies for a wide variety of inorganic and organic compounds, including substituted phenols. For TPQ_{red} the diagonal of the square scheme is determined to be $\Delta G^\circ_{\text{H}\bullet} = 18 \text{ kcal mol}^{-1}$ by subtracting C from the O–H bond dissociation free energy (BDE). To be conservative, the TPQ_{red} was assumed to a BDE = 75 kcal mol^{-1} , comparable to that reported for 4-aminophenol.⁷⁰

Following the square scheme, from right to left and then down, $\Delta G^\circ_{\text{H}\bullet}$ is adjusted by $\Delta G^\circ_{\text{H}^+}$ ($= -RT \ln K_a$), reflecting the pK_a of the semiquinone cation radical TPQ_{sq}H⁺, to obtain the driving-force for ET, ΔG°_{e-} ($= -nFE^\circ$).⁷² Pulse radiolysis studies of the cofactor in solution have indicated a $pK_a \sim 3.4$ for TPQ_{sq}H⁺.³⁹ The value is consistent with our observations that the optical spectrum of the TPQ_{sq} in PSAO does not shift or broaden as the pH is lowered from 10 to 5.5. Conservatively taking the $pK_{a(1)}$ of the TPQ_{sq}H⁺ to be < 5 makes $E^\circ_{(1)} = 0.48 \text{ V vs. NHE}$ a lower limit for the sought after TPQ_{red} one-electron redox potential.

The free energy for outer-sphere ET from reduced PSAO to O₂ can be derived from the difference of $E^\circ(\text{O}_2/\text{O}_2^-) = -0.16 \text{ V vs. NHE}$ and $E^\circ_{(1)}$. In the absence of electrostatic stabilization, the reaction is clearly very unfavorable with $\Delta E^\circ \leq -0.64 \text{ V}$ or $\Delta G^\circ \geq 14.8 \text{ kcal mol}^{-1}$ at 22 °C. Yet $\Delta G^\ddagger = 5.8 \pm 1.3 \text{ kcal mol}^{-1}$ is calculated from $k_{\text{cat}}/K_M(\text{O}_2)$ in PSAO. That the observed barrier is much lower than the lower limit of the calculated thermodynamic barrier argues strongly that outer-sphere ET from the neutral aminoquinol is not a viable mechanism. Though electrostatic stabilization of the O₂•⁻ and/or the TPQ_{sq}•⁺ could make the reaction less unfavorable, it is difficult to envisage how such an interaction could reduce ΔG° by $> 9 \text{ kcal mol}^{-1}$.

The same analysis can be used to evaluate the possibility of outer-sphere electron transfer from the deprotonated aminoquinol. A pK_a of 9.6 has been estimated for the neutral cofactor based on model studies described in **Results** section A.³⁷ Using this value, corresponding to a free energy of $13.15 \text{ kcal mol}^{-1}$, together with the $\Delta G^\circ_{\text{H}\bullet} = 18 \text{ kcal mol}^{-1}$, indicates $\Delta G^\circ_{(2)} = 4.85 \text{ kcal mol}^{-1}$ or $E^\circ_{(2)} = 0.21 \text{ V vs. NHE}$. Solving $E^\circ(\text{O}_2/\text{O}_2^-) - E^\circ_{(2)} = -0.37 \text{ V vs. NHE}$, i.e. $\Delta G^\circ = 8.5 \text{ kcal mol}^{-1}$. This thermodynamic barrier is less unfavorable than for the neutral cofactor but still significantly larger than the observed ΔG^\ddagger . It is certainly possible that enzyme active sites can alter reaction thermodynamics through strategically placed charged residues; though no evidence to this effect has been reported as yet in the copper amine oxidases. In flavoenzymes where outer-sphere ET to O₂ is catalyzed by lowering of the intrinsic reorganization energy (λ), electrostatic stabilization of only $-3.5 \text{ kcal mol}^{-1}$ has been estimated.⁶⁶ Such a stabilization energy in the copper amine oxidases could make ΔG° approximate ΔG^\ddagger , though an additional contribution would still be required to minimize λ and make the kinetic barrier approach 0 kcal mol^{-1} .

In light of the thermodynamics for the resting reduced PSAO, we propose that the presence of Cu^I biases O₂ reduction to proceed by an inner-sphere electron transfer pathway. The Cu–O₂ bond has significant covalent as well as ionic character.¹⁸ Using outer-sphere redox potentials and equilibrium constants for forming Cu–O₂ adducts, the interaction energy of Cu^{II} and O₂•⁻ has been estimated to exceed 25 kcal mol^{-1} .^{8,21} This stabilizing interaction associated with inner-sphere ET upon binding of O₂ to Cu^I is needed to lower ΔG° to the extent necessary to make ΔG^\ddagger comparable to the observed barrier of $5.8 \text{ kcal mol}^{-1}$.

B. The Intrinsic Barrier to O₂ Reduction—Favorable ΔG° , together with pre-organized electrostatics of a protein active site, can result in lowering of the barrier to O₂ reduction. Electrostatic catalysis, where the λ associated with outer-sphere ET to O₂ is dramatically reduced relative to its value in solution, has been described in glucose oxidase⁶⁶ and may exist in many other flavoproteins⁷³ as well as quinoproteins.⁷⁴ Thus, the question arises as to the role of positively charged residues such as the Lys residue conserved among plant amine oxidases.

In PSAO, Lys296 is positioned such that it can lower the pK_a of the amino group in TPQ_{red} and possibly facilitate the deprotonation of the 2 or 4-hydroxyl group through an electrostatic field effect. The formation of TPQ_{red}[−] would be followed by rapid ET to yield the E(Cu^I, TPQ_{sq}) state which we have shown dominates the reduced PSAO at physiological pH. Yet $k_{cat}/K_M(O_2)$ for PSAO is within an order of magnitude of values reported for HPAO⁴² and BSAO⁴⁴ indicating that Lys296 does not dramatically influence the ΔG^\ddagger for O₂ reduction. The residue might, however, alter relevant pK_a values which control ET through the kinetically labile nature of the copper bound water molecules and their propensity for displacement by O₂.

What then causes the rates of copper amine oxidase catalyzed O₂ reduction to exceed those of the analogous un-catalyzed reactions in solution? Several years ago, Merényi and coworkers demonstrated a mechanism of outer-sphere ET from 4-aminophenolate to O₂ that occurs with a rate constant of $7.9 \text{ M}^{-1}\text{s}^{-1}$.⁷⁵ Applying Marcus Theory⁴⁵ indicated $\lambda = 37 \text{ kcal mol}^{-1}$ for this reaction. Assuming for a moment that the same outer-sphere ET mechanism is operative in copper amine oxidases, which exhibits 10⁵-fold rate acceleration, suggests that λ must be lowered on the enzyme by more than 20 kcal mol^{-1} . Yet, in spite of the extensive mutagenesis studies performed on HPAO,^{63,36} none has exposed an amino acid residue which could be considered responsible for this catalytic effect. In one notable active site mutant, D630N HPAO, a rate increase relative to the wild-type enzyme is observed! These results would seem indicative of robustness and plasticity rather than an electrostatically pre-organized active site.⁶⁶

The thermodynamic considerations described above suggest another strategy for lowering the barrier in copper amine oxidase which simply involves inner-sphere ET. The accessibility of the E(Cu^I, TPQ_{sq}) is a critical factor. Most if not all copper amine oxidases^{13,17,42,35,36,44,50} produce the E(Cu^I, TPQ_{sq}) although studies to demonstrate the kinetic competence of the intermediate have only been performed with PSAO¹⁵ and AGAO.³⁵ A critical test of the inner-sphere mechanism in HPAO would involve determining the intra-protein proton-coupled electron transfer rate constants which contribute to K_{int} (cf. Figure 2). It is not until such experiments are performed that we can generalize the observations described in this work to the yeast-derived enzyme.

Nevertheless we point out that the formation of a covalently bound $[\text{Cu}^{\text{II}}(\eta^1\text{-O}_2\text{-}^{\text{I}})]^+$ intermediate derived from the inner-sphere reaction of Cu^I and O₂ would enhance the rate by making ΔG° significantly more favorable than it would be otherwise; noting again $\Delta G^\circ > 14.8 \text{ kcal mol}^{-1}$ is estimated for the outer-sphere reaction between E(Cu^{II}, TPQ_{red}) and O₂. Another possibility, which cannot be discounted, is that the formation of such an intermediate in HPAO is thermodynamically favored yet kinetically disfavored by a coordination inert copper center that blocks the binding of O₂. This type of kinetic barrier to O₂ coordination might be imposed through deprotonation of the copper-bound water. Further, the presence of Cu^{II}OH might also stabilize the anionic aminoquinol with respect to intraprotein ET to the Cu^{II}. We add that in none of the enzymes should the formation of the putative $[\text{Cu}^{\text{II}}(\eta^1\text{-O}_2\text{-}^{\text{I}})]^+$ should not be so far downhill, however, that the intermediate becomes observable using conventional

spectroscopy. Rather the second ET from the TPQ_{sq} appears required to form the Cu^{II}(η^1 -O₂^{-II}) and render O₂ activation irreversible.

IV. Conclusions

These are the first studies to support an inner-sphere electron transfer mechanism during the catalytic reduction of molecular oxygen by copper amine oxidases. Much effort has been devoted to the study of these enzymes from other sources culminating in proposals of partially rate-determining outer-sphere ET from the fully reduced TPQ cofactor to O₂. The findings from the present work provide the first compelling evidence to the contrary and suggest new experiments for some of the systems which have been previously investigated.

Experimental and computational support has been obtained for O₂ binding reversibly to the reduced pea seedling amine oxidase followed by ET from the TPQ semiquinone cofactor in the rate-determining step. More specifically, the evidence for reversible O₂ binding to Cu^I comes from studies of rates as a function pH as well as temperature and the observation of a competitive ¹⁸O KIE, free of kinetic complexity, which falls squarely within the limits expected for an end-on copper superoxide [Cu^{II}(η^1 -O₂^{-I})]⁺ structure and an end-on copper peroxide Cu^{II}(η^1 -O₂^{-II}) structure. The boundary conditions set by superoxide and peroxide structures were calculated by the full set of vibrational frequencies obtained using a recently established density functional method. Thus, the application of a combined experimental/computational approach to analyzing ¹⁸O KIEs upon enzymatic O₂ activation has been successful. The results establish methodology and benchmarks that should be generally useful for identifying kinetically significant metal-oxygen intermediates which are not observable using conventional spectroscopic methods.

In addition to novel mechanistic findings for a plant-derived copper amine oxidase, thermodynamic analyses of the proposed electron transfer reactions have been presented. The results clearly indicate that outer-sphere electron transfer from the fully reduced cofactor to O₂ is highly unfavorable and incompatible with observed free energy barriers for copper amine oxidase-mediated O₂ reduction. The electron transfer from the deprotonated aminoquinol cofactor, a reaction which had not been considered previously, is also unfavorable but less so. Additional experiments will be required to test the kinetic competence of the Cu^I state in the yeast and bovine serum enzymes. If such a state were accessible, the analyses presented herein would suggest O₂ activation by an inner-sphere electron transfer mechanism. This is precisely the proposed mechanism for pea seedling amine oxidase, where O₂ binds directly to Cu^I in the initial moderately favorable to unfavorable step followed by a subsequent rate-determining electron transfer from the TPQ semiquinone to drive the reaction forward. Such inner-sphere ET reactivity may be a strategy exploited by various enzymes, which possess redox active and coordination labile metal centers, to avoid the uncoupled reduction of O₂ and the accumulation of damaging reactive oxygen species during catalysis.

Supplementary Material

Refer to Web version on PubMed Central for supplementary material.

Acknowledgement

J.P.R wishes to acknowledge a National Science Foundation CAREER award CHE-0449900, a Research Corporation Cottrell Scholar Award CS1461 and the Alfred P. Sloan Foundation fellowship. D. M. D. wishes to acknowledge support from the NIH (GM 27659). We also wish to thank Chris Cramer for insightful discussions.

References

1. (a) Janes SM, Mu D, Wemmer D, Smith AJ, Kaur S, Maltby D, Burlingame AL, Klinman JP. *Science* 1990;248:981–987. [PubMed: 2111581] (b) Wang SX, Mure M, Medzihradsky KF, Burlingame AL, Brown DE, Dooley DM, Smith AJ, Kagan HM, Klinman JP. *Science* 1996;273:1078–1084. [PubMed: 8688089] (c) McIntire WS, Hartmann C. *Princ. Appl. Quinoproteins*. Davidson, VL., editor. Dekker; New York: 1993. p. 97–171. (d) Klinman JP. *Proc. Nat. Acad. Sci. USA* 2001;98:14766–14768. [PubMed: 11752422] (e) Mure M. *Acc. Chem. Res* 2004;37:131–139. [PubMed: 14967060]
2. (a) Mondovi B, Pietrangeli P, Morpurgo L, Masini E, Federico R, Mateescu MA, Befani O, Agostinelli E. *Inflammopharmacology* 2003;11:155–163. [PubMed: 15035817] (b) O'Sullivan J, Unzeta M, Healy J, O'Sullivan MI, Davey G, Tipton KF. *Neurotoxicology* 2004;25:303–315. [PubMed: 14697905] (c) Pietrangeli P, Mondovi B. *Neurotoxicology* 2004;25:317–324. [PubMed: 14697906] (d) Toninello A, Pietrangeli P, De Marchi U, Salvi M, Mondovi B. *Biochim. Biophys. Acta, Rev. Cancer* 2006;1765:1–13. (e) O'Sullivan J, Davey G, O'Sullivan M, Tipton KF. *J. Neural Transmiss* 2007;114:751–756.
3. (a) Laurenzi M, Tipping AJ, Marcus SE, Knox JP, Federico R, Angelini R, McPherson MJ. *Planta* 2001;214:37–45. [PubMed: 11762169] (e) Rea G, De Pinto MC, Tavazza R, Biondi S, Gobbi V, Ferrante P, De Gara L, Federico R, Angelini R, Tavladoraki P. *Plant Phys* 2004;134:1414–1426.
4. (a) Harris ED, O'Dell BL. *Adv. Exp. Med. Biol* 1974;48:267–84. [PubMed: 4429037] (b) Langford SD, Trent MB, Boor PJ. *Cardiovascular Toxicology* 2002;2:141–150. [PubMed: 12271157]
5. (a) Klinman JP. *Acc. Chem Res* 2007;40:325–333. [PubMed: 17474709] (b) Bollinger JM, Krebs C. *Curr. Opin. Chem. Biol* 2007;11:151–158. [PubMed: 17374503] (c) Decker A, Solomon EI. *Curr. Opin. Chem. Biol* 2005;9:152–163. [PubMed: 15811799] (d) Valentine JS, Foote CS, Greenberg A, Liebman JF., editors. *Active Oxygen in Biochemistry*. Chapman & Hall; New York: 1995.
6. (a) Xu X, Pin S, Gathinji M, Fuchs R, Harris ZL. *Ann. New York Acad. Sci* 2004;1012:299–305. [PubMed: 15105274] (b) Mukhopadhyay CK, Ehrenwald E, Fox PL. *J. Biol. Chem* 1996;271:14773–14778. [PubMed: 8663020]
7. (a) Valentine JS, Hart PJ. *Proc. Nat. Acad. Sci. USA* 2003;100:3617–3622. [PubMed: 12655070] (b) Valentine JS, Doucette PA, Potter SZ. *Ann. Rev. Biochem* 2005;74:563–593. [PubMed: 15952898] (c) Choi J, Rees HD, Weintraub ST, Levey AI, Chin L-S, Li L. *J. Biol. Chem* 2005;280:11648–11655. [PubMed: 15659387]
8. Taube H. *Prog. Inorg. Chem* 1986;34:607–25.
9. Pietrangeli P, Nocera S, Mondovi B, Morpurgo L. *Biochim. Biophys. Acta, Proteins Proteom* 2003;1647:152–156.
10. Johnson BJ, Cohen J, Welford RW, Pearson AR, Schulten K, Klinman JP, Wilmot CM. *J. Biol. Chem* 2007;282:17767–17776. [PubMed: 17409383]
11. Yamasaki EF, Swindell R, Reed DJ. *Biochemistry* 1970;9:1206–10. [PubMed: 5418714]
12. Mure M, Mills SA, Klinman JP. *Biochemistry* 2002;41:9269–78. [PubMed: 12135347]
13. Dooley DM, McGuirl MA, Brown DE, Turowski PN, McIntire WS, Knowles PF. *Nature* 1991;349:262–264. [PubMed: 1846226]
14. Wilmot CM, Hajdu J, McPherson MJ, Knowles PF, Phillips SE. *Science* 1999;286:1724–1728. [PubMed: 10576737]
15. (a) Kumar V, Dooley DM, Freeman HC, Guss JM, Harvey I, McGuirl MA, Wilce MCJ, Zubak VM. *Structure* 1996;4:943–955. [PubMed: 8805580] (b) Duff AP, Shepard EM, Langley DB, Dooley DM, Freeman HC, Guss JM. *Acta Cryst. F: Struct. Biol. Cryst. Commun* 2006;62:1168–1173.
16. Li R, Klinman JP, Mathews FS. *Structure* 1998;6:293–307. [PubMed: 9551552]
17. Turowski PN, McGuirl MA, Dooley DM. *J. Biol. Chem* 1993;268:17680–2. [PubMed: 8349651]
18. Cramer CJ, Tolman WB. *Acc. Chem. Res* 2007;40:601–608. [PubMed: 17458929]
19. Roth JP. *Curr. Opin. Chem. Biol* 2007;11:142–150. [PubMed: 17307017]
20. (a) Prabhakar R, Siegbahn PEM, Minaev BF, Agren H. *J. Phys. Chem. B* 2004;108:13882–13892. (b) Prabhakar R, Siegbahn PEM, Minaev BF. *Biochim. Biophys. Acta, Proteins Proteom* 2003;1647:173–178.
21. Lanci MP, Smirnov VV, Cramer CJ, Gauchenova EV, Sundermeyer J, Roth JP. *J. Am. Chem. Soc* 2007;129:14697–14709. [PubMed: 17960903]

22. For a leading review that describes the application of heavy atom kinetic isotope effects together with DFT methods see: Schramm VL. *J. Biol. Chem* 2007;282:28297–28300. [PubMed: 17690091]
23. McGuirl MA, McCahon CD, McKeown KA, Dooley DM. *Plant Physiol* 1994;106:1205–1211. [PubMed: 7824646]
24. (a) Medda R, Padiglia A, Bellelli A, Pedersen JZ, Finazzi-Agro A, Floris G. *FEBS Lett* 1999;453:1–5. [PubMed: 10403363] (b) Medda R, Mura A, Longu S, Anedda R, Padiglia A, Casu M, Floris G. *Biochimie* 2006;88:827–835. [PubMed: 16519984]
25. Juda GA, Shepard EM, Elmore BO, Dooley DM. *Biochemistry* 2006;45:8788–8800. [PubMed: 16846222]
26. Brouwer AC, Kirsch JF. *Biochemistry* 1982;21:1302–1307. [PubMed: 7074086]
27. (a) Hasinoff BB, Chishti SB. *Biochemistry* 1982;21:4275–4278. [PubMed: 7126544] (b) Dunford HB, Hasinoff BB. *J. Inorg. Biochem* 1986;28:263–269. [PubMed: 3027256]
28. Roth, JP.; Klinman, JP. *Isotope Effects in Chemistry and Biology*, Kohen, A.; Limbach, H-H., editors. CRC Press; Boca Raton: 2006. p. 645–669. (b) Smirnov VV, Brinkley DW, Lanci MP, Karlin KD, Roth JP. *J. Mol. Catal. A* 2006;251:100–107.
29. Frisch, MJ., et al. *Gaussian 03*. Gaussian, Inc.; Pittsburgh, PA: 2003.
30. (a) Perdew JP, Wang Y. *Phys. Rev. B* 1986;33:8800–8802. Perdew, JP. *Electronic Structure of Solids '91*. Ziesche, P.; Eschrig, H., editors. Akademie Verlag; Berlin: 1991. p. 11–20. (c) Adamo C, Barone V. *J. Chem. Phys* 1998;108:664–675.
31. Hehre, WJ.; Radom, L.; Schleyer, PR.; Pople, JA. *Ab Initio Molecular Orbital Theory*. Wiley; New York: 1986.
32. Stevens WJ, Krauss M, Basch H, Jasien PG. *Can. J. Chem* 1992;70:612–629.
33. Cramer, CJ. *Essentials of Computational Chemistry*. 2nd Ed.. Wiley; Chichester: 2004.
34. Details are provided as **Supporting Information**.
35. Shepard EM, Juda GA, Ling K-Q, Sayre LM, Dooley DM. *J. Inorg. Biochem* 2004;9:256–268.
36. Welford RWD, Lam A, Mirica LM, Klinman JP. *Biochemistry* 2007;46:10817–27. [PubMed: 17760423]
37. Mure M, Klinman JP. *J. Am. Chem. Soc* 1993;115:7117–27.
38. Tripathi GNR. *J. Chem. Phys* 2003;118:1378–1391.
39. Bisby RH, Johnson SA, Parker AW. *J. Phys. Chem. B* 2000;104:5832–5839.
40. (a) Cleland WW. *Adv. Enzymol. Relat. Areas Mol. Biol* 1977;45:273–387. [PubMed: 21524] (b) Renard M, Fersht AR. *Biochemistry* 1973;12:4713–4718. [PubMed: 4773852]
41. Melander, L.; Saunders, WH, Jr.. *Reaction Rates of Isotopic Molecules*. Wiley & Sons; New York: 1980. p. 22
42. Mills SA, Goto Y, Su Q, Plastino J, Klinman JP. *Biochemistry* 2002;41:10577–10584. [PubMed: 12186541]
43. Pietrangeli P, Federico R, Mondovi B, Morpurgo L. *J. Inorg. Biochem* 2007;101:997–1004. [PubMed: 17521737]
44. Su Q, Klinman JP. *Biochemistry* 1998;37:12513–12525. [PubMed: 9730824]
45. Marcus RA, Sutin N. *Biochim. Biophys. Acta* 1985;811:265–322.
46. (a) Hartmann C, Brzovic P, Klinman JP. *Biochemistry* 1993;32:2234–41. [PubMed: 8443165] (b) Hartmann C, Dooley DM. *Methods in Enzymology* 1995;258:69–90. [PubMed: 8524165]
47. Mure M, Klinman JP. *J. Am. Chem. Soc* 1995;117:8707–8718.
48. Takahashi K, Klinman JP. *Biochemistry* 2006;45:4683–4694. [PubMed: 16584203]
49. (a) Smirnov VV, Roth JP. *J. Am. Chem. Soc* 2006;128:16424–16425. [PubMed: 17177351] (b) Smirnov VV, Roth JP. *J. Am. Chem. Soc* 2006;128:3683–3695. [PubMed: 16536541]
50. (a) Bellelli A, Agro AF, Floris G, Brunori M. *J. Biol. Chem* 1991;266:20654–7. [PubMed: 1939114] (b) Medda R, Padiglia A, Bellelli A, Sarti P, Santanche S, Finazzi-Agro A, Floris G. *Biochem. J* 1998;332:431–437. [PubMed: 9601072]
51. Mills SA, Klinman JP. *J. Am. Chem. Soc* 2000;122:9897–9904.
52. Cotton, FA.; Wilkinson, G. *Advanced Inorganic Chemistry*. 5th Ed.. Wiley & Sons; New York: 1988. p. 732–733.

53. Roth JP, Wincek R, Nodet G, Edmondson DE, McIntire WS, Klinman JP. *J. Am. Chem. Soc* 2004;126:15120–15131. [PubMed: 15548009]
54. Shepard EM, Dooley DM. *J. Biol. Inorg. Chem* 2006;11:1039–1048. [PubMed: 16924556]
55. The factor of 2.4 is estimated by assuming that O₂ reacts preferentially with the E(Cu^I, TPQ_{sq}) and considering the total enzyme concentration given by: $[E]_T = [E(Cu^I, TPQ_{sq})] + [E(Cu^{II}, TPQ_{red})] = [E(Cu^I, TPQ_{sq})](K_{int} + 1/K_{int})$ where $K_{int} = 5.9$ at pH 6 and 0.48 at pH 10.
56. Duff AP, Trambaiolo DM, Cohen AE, Ellis PJ, Juda GA, Shepard EM, Langley DB, Dooley DM, Freeman HC, Guss JM. *J. Mol. Biol* 2004;344:599–607. [PubMed: 15533431]
57. Mura A, Anedda R, Pintus F, Casu M, Padiglia A, Floris G, Medda R. *FEBS J* 2007;274:2585–2595. [PubMed: 17433047]
58. Similar intrinsic isotope effects upon C–H, containing small contributions from deuterium in the secondary position, have been reported for BSAO: (a) Farnum M, Palcic M, Klinman JP. *Biochemistry* 1986;25:1898–1904. [PubMed: 3518796] (b) Grant KL, Klinman JP. *Biochemistry* 1989;28:6597–605. [PubMed: 2790014] Significantly larger kinetic isotope effects have been reported in AGAO. Murakawa T, Okajima T, Kuroda S, Nakamoto T, Taki M, Yamamoto Y, Hayashi H, Tanizawa K. *Biochem. Biophys. Res. Comm* 2006;342:414–423. [PubMed: 16487484]
59. Loftfield RB, Eigner EA, Pastuszyn A, Lovgren TN, Jakubowski H. *Proc. Nat. Acad. Sci. USA* 1980;77:3374–8. [PubMed: 6932025]
60. Dooley DM, Scott RA, Knowles PF, Colangelo CM, McGuirl MA, Brown DE. *J. Am. Chem. Soc* 1998;120:2599–2605.
61. Lanci MP, Roth JP. *J. Am. Chem. Soc* 2006;128:16006–7. [PubMed: 17165732]
62. (a) Wang M-YR, Hoffman BM, Shire SJ, Gurd FRN. *J. Am. Chem. Soc* 1979;101:7394–7. (b) Walker FA. *J. Am. Chem. Soc* 1973;95:1154–9. [PubMed: 4347146]
63. Goto Y, Klinman JP. *Biochemistry* 2002;41:13637–13643. [PubMed: 12427025]
64. (a) Tilton RF Jr, Singh UC, Weiner SJ, Connolly ML, Kuntz ID Jr, Kollman PA, Max N, Case DA. *J. Mol. Biol* 1986;192:443–56. [PubMed: 3560222] (b) Tilton RF Jr, Kuntz ID Jr. *Biochemistry* 1982;21:6850–7. [PubMed: 7159568] (c) Ewing GJ, Maestas S. *J. Phys. Chem* 1970;74:2341–4. [PubMed: 5445459]
65. Steinbach PJ, et al. *Biochemistry* 1991;30:3988–4001. [PubMed: 2018767]
66. Roth JP, Klinman JP. *Proc. Natl. Acad. Sci. USA* 2002;100:62–67. [PubMed: 12506204]
67. Lanci MP, Brinkley DW, Stone KL, Smirnov VV, Roth JP. *Angew. Chem., Int. Ed* 2005;44:7273–7276.
68. Cramer CJ, Tolman WB, Theopold KH, Rheingold AL. *Proc. Natl. Acad. Sci. USA* 2003;100:3635–3640. [PubMed: 12634422]
69. Scarpellini M, Neves A, Hoerner R, Bortoluzzi AJ, Szpoganics B, Zucco C, Silva Rene A. N. Drago V, Mangrich AS, Ortiz WA, Passos WAC, De Oliveira MCB, Terenzi H. *Inorg. Chem* 2003;42:8353–8365. [PubMed: 14658888]
70. Bordwell FG, Cheng J. *J. Am. Chem. Soc* 1991;113:1736–43.
71. Mayer, JM. *Biomimetic Oxidations Catalyzed by Transition Metal Complexes*. Meunier, B., editor. Imperial College Press; London: 2000. p. 1–43.
72. The n represents the number of electrons transferred and F is Faraday's constant = 23.06 kcal mol⁻¹/V.
73. Massey V. *Int. Congr. Ser* 2002;1233:3–11.
74. Klinman JP. *J. Biol. Inorg. Chem* 2001;6:1–13. [PubMed: 11191216]
75. Merényi G, Lind J, Jonsson M. *J. Am. Chem. Soc* 1993;115:4945–4946.

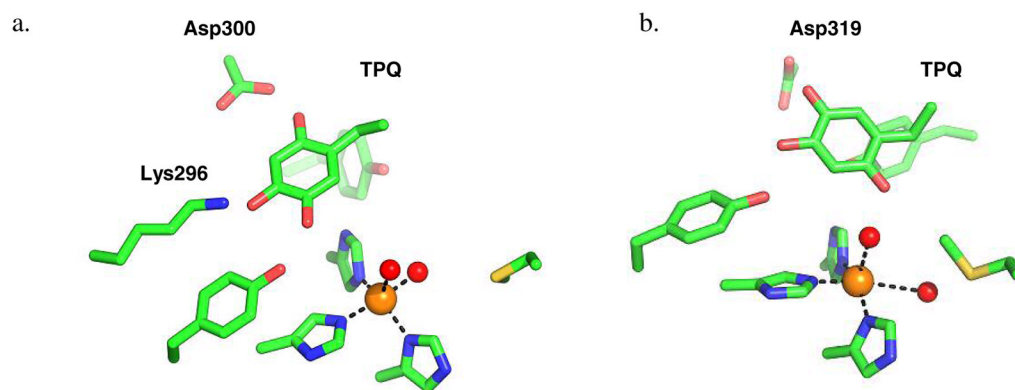


Figure 1. Oxidized forms of copper amine oxidase from pea seedling¹⁵ (a) and *H. polymorpha*¹⁶ (b).

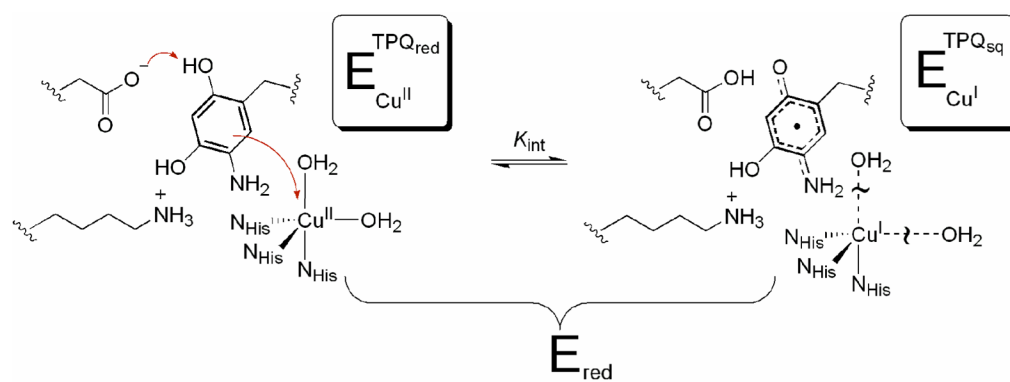
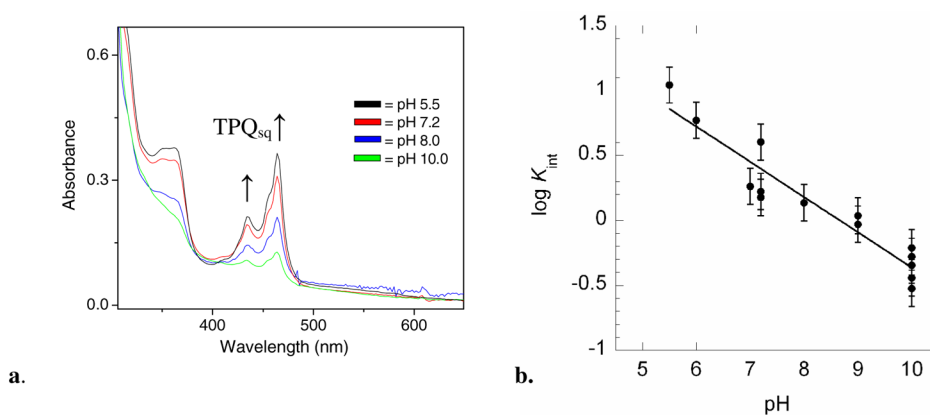
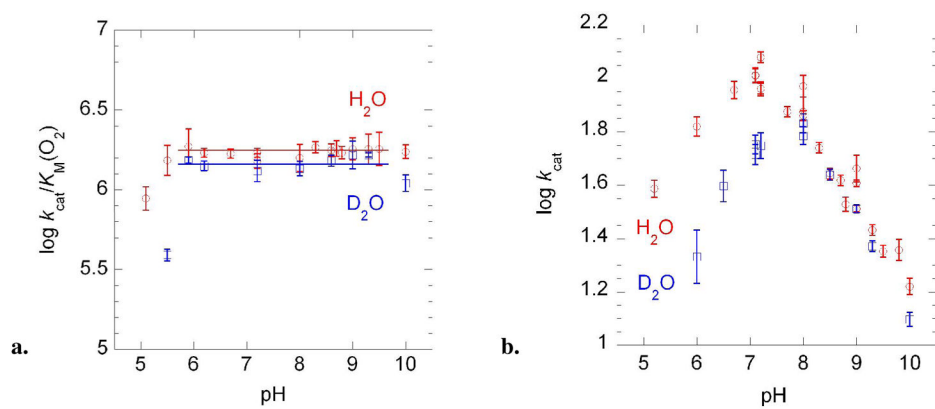


Figure 2.
The redox equilibrium in reduced PSAO (E_{red}) involving proton-coupled electron transfer.

**Figure 3.**

(a) Redox titration of PSAO showing formation of TPQ_{sq} under anaerobic conditions. (b) The pH dependence of K_{int} (cf. Figure 2) corresponding to production of E(Cu^I, TPQ_{sq}) at 22 °C, $\mu = 0.1$ M.

**Figure 4.**

Profiles of (a) $k_{\text{cat}}/K_M(\text{O}_2)$ and (b) k_{cat} at 22 °C (H_2O , red circles), (D_2O , blue squares). The ionic strength was maintained in all experiments ($\mu = 0.1 \text{ M}$).

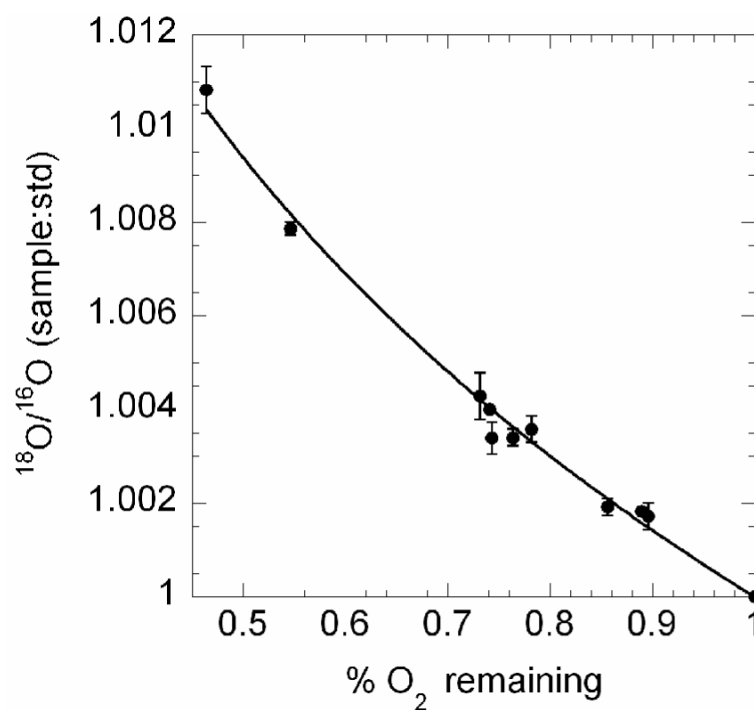


Figure 5.
Oxygen isotope fractionation during PSAO turnover at pH 7.2 and 22 °C, $\mu = 0.1$ M.

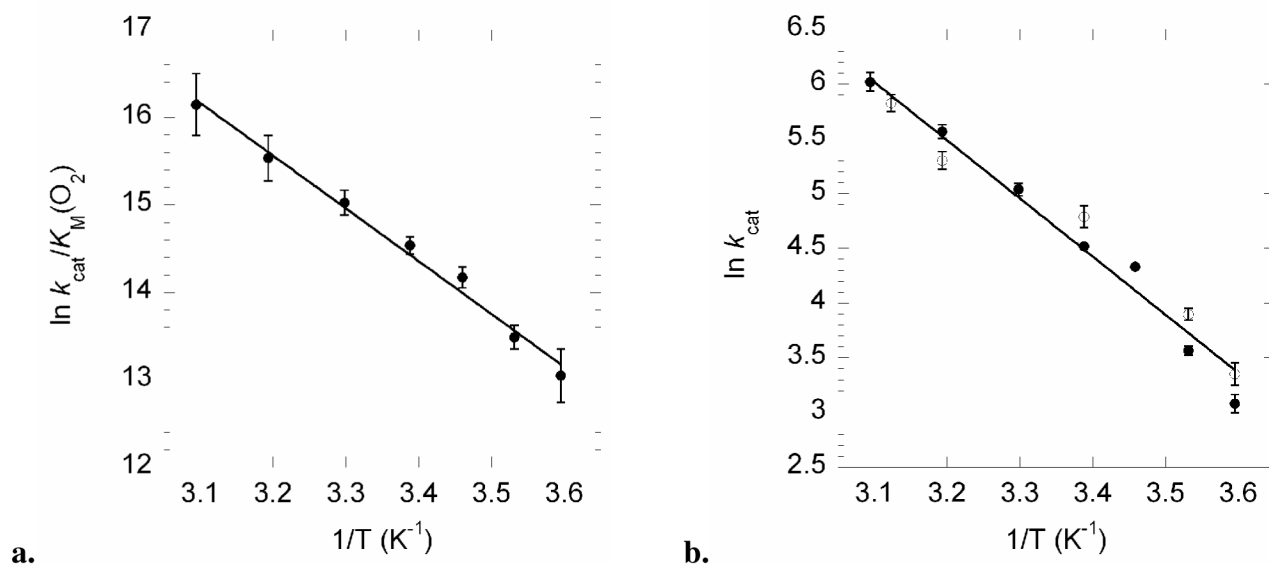


Figure 6.

Activation parameters for putrescine oxidation at pH 7.2 ($\mu = 0.1\text{M}$): (a) the temperature dependence of (a) $k_{\text{cat}}/K_{\text{M}}(\text{O}_2)$ and (b) k_{cat} . The k_{cat} values were determined by varying amine (open circles) or varying O_2 (closed circles). Error bars are $\pm 2\sigma$.

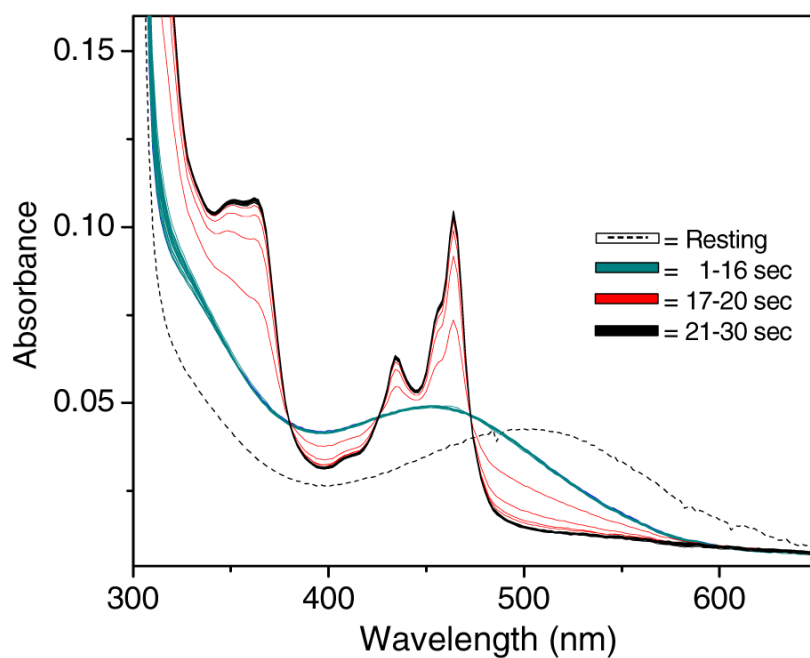
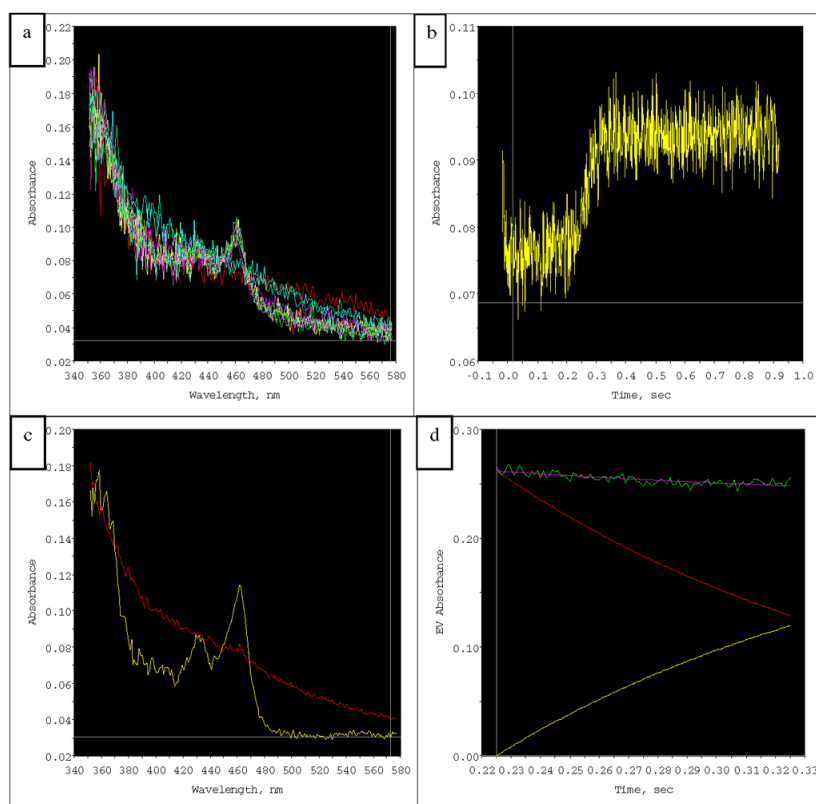
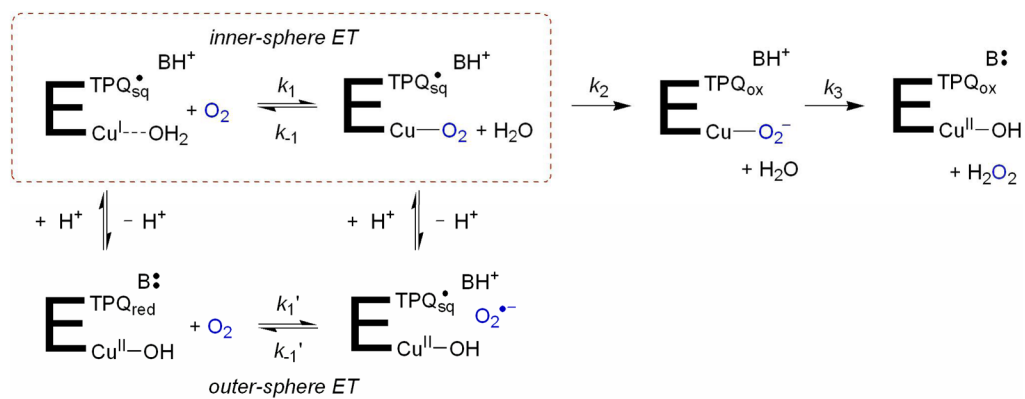


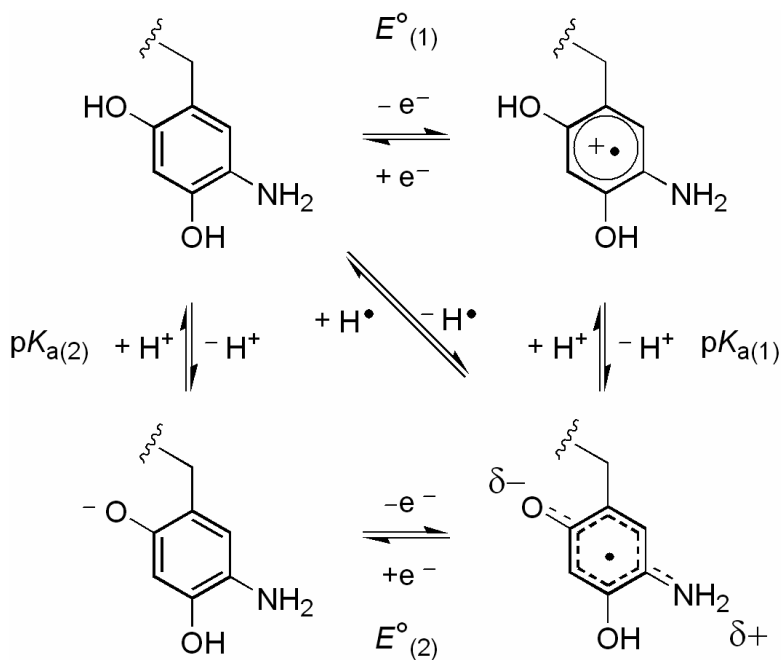
Figure 7.
Steady-state accumulation of the product Schiff-base at pH 7.2, $\mu = 0.5$ M and 20°C.

**Figure 8.**

The approach to steady-state in the reaction of PSAO (10 μM) with O_2 (1.0 mM) and putrescine (5 mM) at pH 7.2, $\mu = 0.1\text{M}$ and 24°C . (a) Overlay of spectra collected over 1 s. (b) The absorbance change at 462nm. (c) The initial and final calculated spectra (see text for details). (d) The changes in concentration corresponding to the initial and final spectra in (c).

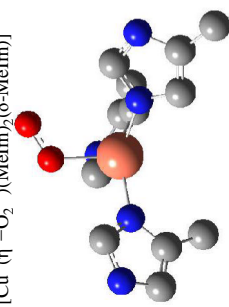
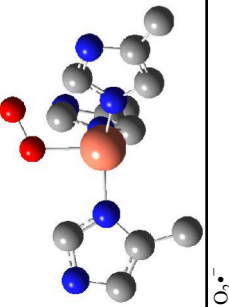
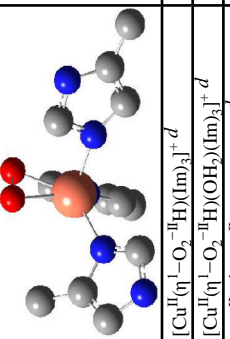
**Scheme 1.**

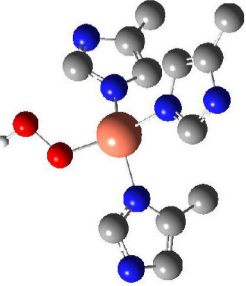
Kinetic mechanism for the oxidative half-reaction of PSAO.

**Scheme 2.**

Thermodynamic cycle for assessing the driving-force for TPQ_{red} oxidation.

Table 1
Energy minimized structures used to compute equilibrium oxygen isotope effects (^{18}O EIEs).

	Structure ^a	$\nu(^{16}\text{O}-^{16}\text{O})$ (cm^{-1})	$d(\text{O}-\text{O})$ (\AA)	^{18}O EIE _{max} ($\text{O}_2 \rightarrow \text{product}$) ^f	^{18}O EIE (22 °C)
1	O_2	1550	1.221	—	—
2	$[\text{Cu}^{\text{II}}(\eta^1\text{-O}_2^{-1})(\text{Im})_3]^+{}^b$	1342	1.257	1.0108 (−70 °C)	1.0092
3	$[\text{Cu}^{\text{II}}(\eta^1\text{-O}_2^{-1})(\text{OH}_2)(\text{Im})_3]^+{}^b$	1249	1.285	1.0095 (24 °C)	1.0095
4	$[\text{Cu}^{\text{II}}(\eta^1\text{-O}_2^{-1})(\text{MeIm})_3]^+{}^b$	1339, 1343	1.250	1.0104 (−70 °C)	1.0092
5	$[\text{Cu}^{\text{II}}(\eta^1\text{-O}_2^{-1})(\text{MeIm})_2(\delta\text{-MeIm})]^+{}^c$				
		1341, 1344	1.256	1.0107 (−79 °C)	1.0094
6	$\text{Cu}^{\text{II}}(\eta^1\text{-O}_2^{-1})(\text{Im})_3$ ^d	1124.8	1.350	1.0308 (−144 °C)	1.0214
7	$\text{Cu}^{\text{II}}(\eta^1\text{-O}_2^{-1})(\text{Im})_3 \cdot \text{H}_2\text{O}$ ^{d,e}	1088, 1107	1.355	1.0196 (−62 °C)	1.0178
8	$\text{Cu}^{\text{II}}(\eta^1\text{-O}_2^{-1})(\text{MeIm})_3$ ^d	1114	1.355	1.0275 (−125 °C)	1.0209
9	$[\text{Cu}^{\text{II}}(\eta^1\text{-O}_2^{-1})(\text{MeIm})_2(\delta\text{-MeIm})]$ ^{c,d}				
		1069	1.366	1.0340 (−139 °C)	1.0240
10	$\text{O}_2^{\bullet -}$	1097	1.363	$\rightarrow \infty$ (−273 °C) ^g	1.0310
11	$\text{Cu}^{\text{II}}(\eta^2\text{-O}_2^{-1})(\text{Im})_3$ ^d	997	1.403	1.0631 (−209 °C)	1.0313
12	$\text{Cu}^{\text{II}}(\eta^2\text{-O}_2^{-1})(\text{Im})_3 \cdot \text{H}_2\text{O}$ ^{d,e}	956	1.427	1.0359 (−136 °C)	1.0272
13	$\text{Cu}^{\text{II}}(\eta^2\text{-O}_2^{-1})(\text{MeIm})_3$ ^d	988	1.400	1.0643 (−199 °C)	1.0313
14	$[\text{Cu}^{\text{II}}(\eta^2\text{-O}_2^{-1})(\text{MeIm})_2(\delta\text{-MeIm})]$ ^{c,d}				
		973, 978	1.416	1.0559 (−181 °C)	1.0311
15	$[\text{Cu}^{\text{II}}(\eta^1\text{-O}_2^{-1})(\text{H})(\text{Im})_3]^+{}^d$	899	1.428	1.0145 (−29 °C)	1.0139
16	$[\text{Cu}^{\text{II}}(\eta^1\text{-O}_2^{-1})(\text{H})(\text{OH})(\text{Im})_3]^+{}^d$	886, 852	1.447	1.0114 (23 °C)	1.0114
17	$[\text{Cu}^{\text{II}}(\eta^1\text{-O}_2^{-1})(\text{H})(\text{MeIm})_3]^+{}^d$	911	1.421	1.0118 (−1 °C)	1.0117

Structure ^d	$\nu(^{16}\text{O}-^{16}\text{O})$ (cm^{-1})	$d(\text{O}-\text{O})$ (\AA)	^{18}O EIE _{max} ($\text{O}_2 \rightarrow \text{product}$) ^f	^{18}O EIE (22 °C)
18 [Cu ^{II} (η^1 -O ₂ - ¹⁸ H)(MeIm) ₂ (δ -MeIm)] ⁺ c,d 	900	1.424	1.0127 (−8 °C)	1.0125

^a Formal oxidation states are assumed. Entries 6-9 can be reformulated as Cu^I(η^1 -O₂^{−1}) based on the increased copper character in the SOMO. Details are provided in the supporting information.

^b A triplet ground state is assumed.²¹

^c δ -MeIm denotes that the methylimidazole ligand was constrained to coordinate through the δ -nitrogen adjacent to the methyl group.

^d Doublet ground state.

^e The water molecule is dissociated from the copper yet hydrogen bonded to the terminal oxygen of the peroxide ligand.

^f The approximate temperature at which the ^{18}O EIE passes through a maximum is given in parentheses.

^g The EIE approaches infinity as the temperature approaches absolute 0.